USING ARTIFICIAL NEURAL NETWORK AND SEQUENTIAL PREDICTIVE PROBABILITY METHOD TO MECHANIZE INTERPRETATION OF WELL TEST DATA

A REPORT
SUBMITTED TO THE DEPARTMENT OF PETROLEUM ENGINEERING
OF STANFORD UNIVERSITY
IN PARTIAL FULFILLMENT OF THE REQUIREMENTS
FOR THE DEGREE OF
MASTER OF SCIENCE

By
Suwat Athichanagorn
June 1995

I certify that I have read this report and that in my opinion it is fully adequate, in scope and in quality, as partial fulfillment of the degree of Master of Science in Petroleum Engineering.

Dr. Roland Horne
(Principal advisor)

Abstract

We propose a robust way of achieving a well test interpretation by combining the sequential predictive probability method with an artificial neural network approach. The sequential predictive probability method considers all possible reservoir models and determines which candidate model or models best predict the well response. This method is dependent on obtaining good initial estimates for the parameters governing the candidate reservoir models, which is achieved by applying the artificial neural network approach. We use the neural network to identify the characteristic components of the pressure derivative curve corresponding to the flow regimes known to be in each candidate model. Reservoir parameters are then computed using the data in the identified range of the corresponding behavior.

As a final step, the candidate models and their initial estimates are evaluated using the sequential probability method. The method discriminates between the candidate models and simultaneously performs nonlinear regression to compute the best estimates of reservoir parameters.

The trained neural network was able to identify the characteristic components of the derivative curve in most cases. The algorithm written to interpret the neural network signals into flow regimes required special procedures to take care of the misclassification from the neural network. The initial estimates of reservoir parameters from the neural network were found to be reasonably close to the eventual estimates from the sequential predictive probability method.

Acknowledgements

I would like to express my deep gratitude to Professor Roland N. Horne for his guidance and advice throughout the entire course of this study. His profound knowledge and experience have made this work possible. The financial support provided by Stanford University Petroleum Research Institute (SUPRI-D) is gratefully acknowledged.

Contents

List of Tables

List of Figures

Section 1

Introduction

Traditional methods of well test interpretation are usually based on a combination of manual and automated techniques, although both techniques are usually computer based. Manual interpretation uses the pressure derivative plot introduced by Bourdet, Whittle, Douglas and Pirard (1983). The characteristics of different reservoir flow regimes can be observed from the plot. Hence, we are able to analyze the type of the associated reservoir and determine their parameters from the appropriate flow regimes. Automated interpretation by nonlinear regression is then used to determine the best estimates of reservoir parameters, and confidence intervals are used to authenticate the selected reservoir model.

With new developments in pressure measurement, including permanently installed gauges, we may have an enormous amount of pressure data coming in each day. This study looked at a procedure to mechanize the interpretation of such well test data. There are three key steps in the procedure. First, all the characteristic components of the pressure derivative plot have to be recognized. This task is accomplished by a specially trained artificial neural network. Second, the signals from the neural network are translated into reservoir flow regimes so that initial estimates of reservoir parameters can be evaluated. Third, the sequential predictive probability discriminates between candidate reservoir models, simultaneously performing nonlinear regression based on the initial estimates provided by the neural network.

Section 2 of this report outlines a list of related work that has been previously

conducted.

Section 3 describes the principle of artificial neural networks in general and their application in identifying characteristic components of the pressure derivative plot. The procedure in the sequential predictive probability method is also presented.

Section 4 discusses the interpretation of the neural network signals into reservoir flow regimes and procedures used to determine initial estimates of reservoir parameters.

Section 5 demonstrates the application of the coupling between the the neural network and the sequential predictive probability method. Three sets of actual field tests and three sets of simulated tests are analyzed.

Section 6 summarizes the approach taken in this study. Several remarks are made in applying this approach to mechanize the well test interpretation.

Section 2

Previous Work

There have been several attempts over the past few years to mechanize the interpretation of well test data. This section discusses some of these related works.

Allain and Horne (1990) used syntactic pattern recognition and a rule-based system to identify the reservoir model and to estimate its parameters. The pressure derivative data were first preprocessed in order to distinguish the true response from the noise. This task corresponds to the construction of a sketch which contains symbolic shapes (up, down, maximum, minimum, plateau, and valley). The rule-based system then used the existing symbols to create potential reservoir models. Finally, reservoir parameters were estimated using the regimes in the model description and the segments in the sketch of the derivative. It was found that the derivative curve may need to be smoothed if the data were noisy. The disadvantage of this approach is that it requires a preprocessing of the derivative data and a complex definition of rules to accommodate nonideal behavior.

Al-Kaabi and Lee (1990) used artificial neural networks to identify the well test interpretation model from pressure derivative data. The neural networks were trained on examples of derivative plots from several reservoir models. The authors reported that the neural network was effective in identifying reservoir models and data smoothing is unnecessary due to the generalization of neural network understanding. However, this work provides only a qualitative description of the well test. The computation of reservoir parameters was not considered.

Seeing the shortcomings of the artificial neural network approach as a tool in well test interpretation, Ershaghi, Li and Hassibi (1993) implemented multiple neural networks with each neural network representing a single reservoir model to overcome the inefficiency in the training of an enormous number of reservoir models. This approach improved the full representation of each reservoir model. However, parameter estimation was not mentioned in their work.

Recognizing the advantages and disadvantages of the symbolic and artificial neural network methods, Allain and Houzé (1992) proposed a hybrid approach to combine the two methods. Since model identification and parameter estimation requires visual recognition and reasoning ability, they suggested that the neural network approach be used for the visual recognition and that the symbolic approach be used for the reasoning part. In essence, they proposed to use the neural network to determine the sketch of the derivative before applying a rule-based approach to determine the model and estimate its parameters.

Recently, Anraku and Horne (1993) introduced a new approach to discriminate between reservoir models using the sequential predictive probability method. This approach was effective in identifying the correct reservoir models by matching to all candidate reservoir models and then computing the probability that each match would correctly predict the pressure response. Candidate reservoir models and initial estimates of the models' parameters need to be determined in advance for this process.

We investigated the use of the neural network to recognize characteristic components of candidate models on the derivative plot (unit slope, hump, flat slope, dip, and descending shape) so that reservoir flow regimes corresponding to these characteristic components and their underlying parameters would be identified. These parameter estimates are not intended to be used as final answers but as initial guesses to pass to the sequential predictive probability algorithm. The application of the sequential predictive probability program (Anraku 1993) avoids the need to construct reservoir models from the components of the derivative identified by the neural network and hence overcomes the difficulty of nonideal responses. The sequential predictive probability program identifies the reservoir model out of a suite of possible candidates and at the same time evaluates the best estimates of the unknown reservoir parameters.

Section 3

Artificial Neural Network

There has been a tremendous growth of interest in artificial neural networks and their applications over the past recent years. Neural networks are very powerful tools for solving several types of problems, but most commonly they are used to solve pattern classification (or mapping) problems such as speech recognition, hand writing recognition, and stock market prediction.

This section first explains the principle of the artificial neural networks and then discusses the implementation of the artificial neural network approach to reservoir flow regime characterization from well test data. Typical patterns of various flow regimes that can be observed from the pressure derivative plot are investigated. We further show the architecture of the artificial neural network trained in this study to recognize basic flow regimes and discusses several points concerning neural network training. Candidate reservoir models to be used in the sequential predictive probability method are also presented since the identifiable component of these models represent the output targets for the neural network.

3.1 Principle

An artificial neural network is an information-processing system that has certain performance characteristics in common with biological neural networks (Fausett, 1994). The approach is based on the belief that intelligence is achieved through interaction

between large number of processing units or artificial neurons (Wasserman 1989). Fausett summarizes the assumptions made in the development of artificial neural networks as generalizations of mathematical models of human cognition or neural biology as follows:

1. Information processing occurs at many simple elements called neurons.
2. Signals are passed between neurons over connection links.
3. Each connection link has an associated weight, which, in a typical neural net, multiplies the signal transmitted.
4. Each neuron applies an activation function (usually nonlinear) to its net input (sum of weighted input signals) to determine its output signal.

These assumptions are developed from the anatomical understanding of the brain which contains billions of elementary units called neurons. The three most important components of a neuron are soma, dendrites, and axon. The dendrites are irregularly shaped filaments branching from the soma, which is the cell body. They receive signals from other neurons. These signals are electric impulses that are transmitted across a synaptic gap by a chemical process. The action of the chemical transmitter modifies (strengthens or weakens) the incoming signals in a way similar to the action of the weights in the artificial neural network. The soma sums the modified incoming signals. If enough input signals are received, the neuron becomes activated and fires a signal over its axon, which serves as the output channel of the neuron.

It is thought that learning occurs when the chemical transmitters adjust the connections between neurons (Beale and Jackson, 1990). This is the key concept in the artificial neural network procedure. The learning in the artificial neural network is accomplished by adjusting the weights connecting a threshold of processing units.

Al-Kaabi and Lee (1990) summarizes the artificial neural network system architecture and the learning algorithm used to train the network. Figure 3.1 shows a schematic diagram of a multilayer artificial neural network. This specific neural network is a three layered neural net. Each layer consists of several processing units

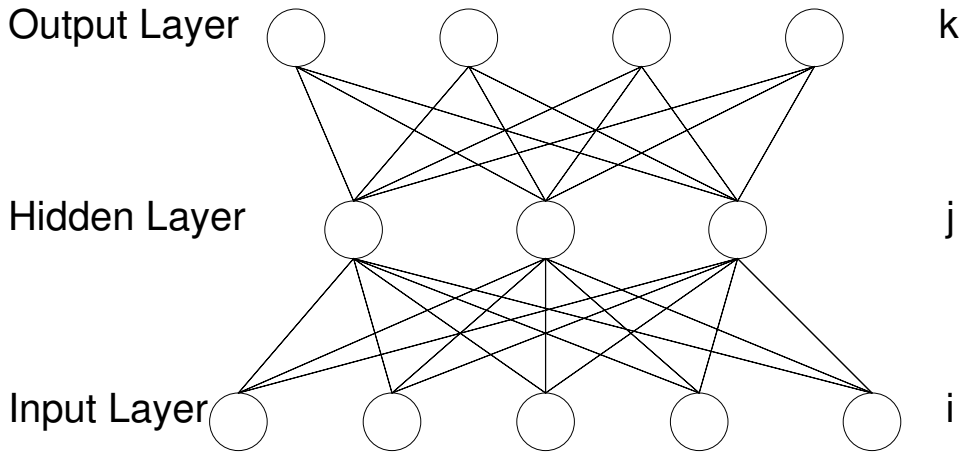

Figure 3.1: Schematic diagram of multilayer artificial neural network

(nodes). The first (bottom) layer is an input layer where the input data are entered. The second layer is called a hidden layer or a middle layer, and the last (top) layer is an output layer. The processing units in each layer are connected to those in the adjacent layers. These connections are called links. Each link has a weight which can be a positive or negative number associated with it. The links are strong when the weights are positive and weak when the weights become negative. The activation level, which is an output signal from each processing unit in the second and third layers, is determined by a thresholding function called the squashing or activation function. This function is nonlinear, continuous, differentiable everywhere and has a sigmoidal shape. It reaches the value 1 when the argument is a very large positive number and reaches the value 0 when the argument is a very small negative number. A typical thresholding function used in the neural network is depicted in Figure 3.2 and described by the following equation:

$$O_j = \frac{1}{1 + exp(-net_j)} \tag{3.1}$$

where O_j is the output from a processing unit in the j-th layer and net_j is the weighted sum of the all the outputs from the processing units in the previous layer expressed

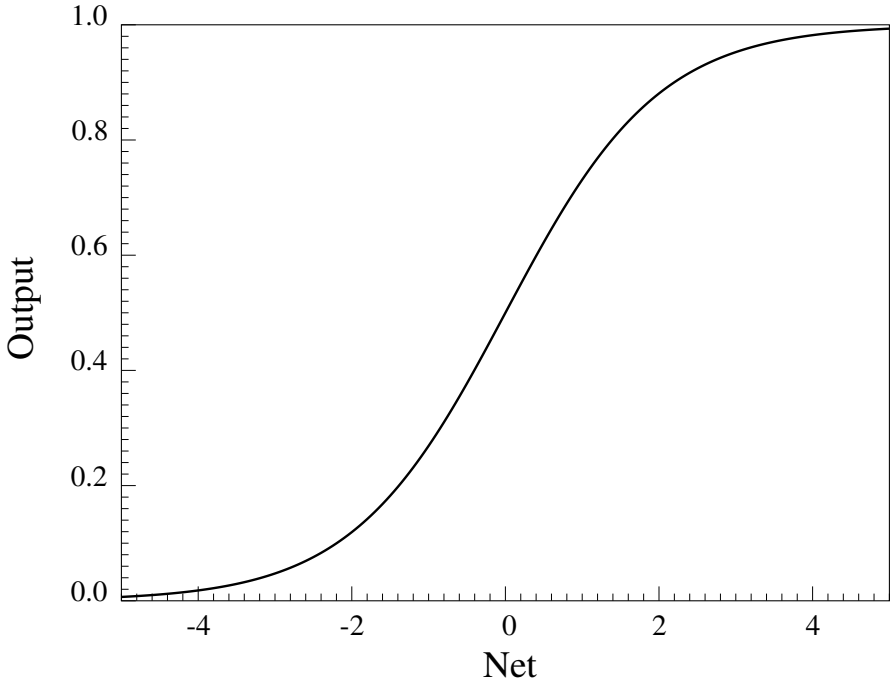

Figure 3.2: Thresholding function

by the following equation:

$$net_j = \sum_{i=1} w_{ji} O_i \tag{3.2}$$

where w_{ji} is the weight associated with the link between a processing unit in the i-th layer and a processing unit in the j-th layer and O_i is the output of a processing unit in the i-th layer.

The neural network learns to perform tasks (in most cases, classify patterns) from a set of examples. Each example contains an input vector and an output vector (sometimes called a teaching vector). The most frequently used learning (or training) algorithm is the backpropagation algorithm. In this algorithm, the error (which is the difference between the computed output and the actual output) is propagated back to the neural network and used to adjust each weight in the next iteration. Each weight is adjusted proportionally to the amount of error it brings to the output layer.

In order to generalize the neural network understanding, another set of data are used to test the accuracy of the neural network prediction during the training process. These data are called testing data. The high accuracy in the output prediction of the training data itself is not sufficient to guarantee the generalization of the neural network. The testing data should cover all possible cases in order to ensure that we achieve generalization. The training is considered successful if the accuracies of the training and testing outputs meet preset standards. Then, the trained neural network can be used to perform the task it is trained for.

3.2 Using Artificial Neural Network to Identify Reservoir Flow Regimes

The pressure derivative plot is the most useful plot in analyzing the reservoir response during a well test. Reservoir flow regimes can be determined by investigating the shape of the derivative plot in both buildup and drawdown tests. Reservoir parameters can be computed using the pressure data in the appropriate flow regimes. Table 3.1 summarizes the characteristics of the pressure derivative and the pressure change itself and additional distinguishing characteristics for different flow regimes (Economides, Hill, and Ehlig-Economides, 1994). In practice, these characteristics should appear for a period of at least one log cycle in order to be interpreted as flow regimes. If they are shorter than one log cycle, they are probably noise or transitions between flow regimes.

An artificial neural network can be trained to recognize these distinct characteristics of the flow regimes. In this study, a neural network was trained to recognize eight different patterns as follows:

1. flat slope pattern
2. unit slope pattern
3. 1/4 slope pattern
4. 1/2 slope pattern

Table 3.1: Characteristics of pressure derivative for common flow regimes.

Flow Regime	Pressure Change Slope	Pressure Derivative Slope	Additional Distinguishing Characteristic
Wellbore Storage (WBS)	1	1	early time pressure change and derivative are overlain
Finite Conductivity Vertical Fracture (FCVF)	1/4	1/4	early time (after WBS) pressure change and derivative are offset by a factor of 4
Infinite Conductivity Vertical Fracture (ICVF)	1/2	1/2	early time (after WBS and/or FCVF) pressure change and derivative are offset by a factor of 2
Partial Penetration (PPEN)	leveling off	-1/2	middle time (after WBS and before IARF)
Infinite Acting Radial Flow (IARF)	increasing	0	middle time flat derivative
Dual Porosity with Pseudo-Steady State Interporosity Flow	increasing, leveling off, increasing	0, dip, 0	middle time valley trend; duration is more than one log cycle
Dual Porosity with Transient Interporosity Flow	steepening	0, upward trend, 0	middle time slope doubles
Single Sealing Fault	steepening	0, upward trend, 0	late time slope doubles
Elongated Reservoir	1/2	1/2	late time pressure change and derivative are offset by a factor of 2; slope of 1/2 occurs much earlier in the derivative
Pseudosteady State	1 for drawdown; 0 for buildup	1 for drawdown; steeply descending for buildup	late time drawdown pressure change and derivative are overlain; slope of 1 occurs much earlier in the derivative
Constant Pressure Boundary	0	steeply descending	cannot be distinguished from pseudosteady state in pressure buildup data

5. -1/2 slope pattern

6. hump pattern

7. dip (valley) pattern

8. descending pattern

The flat slope pattern is used to characterize infinite acting radial flow and single sealing fault flow regimes. The unit slope patterns at early time and late time are used to find wellbore storage and pseudosteady state flow regimes, respectively. A finite conductivity vertical fracture flow regime can be identified by the presence of the one quarter slope pattern. The one half slope pattern can be used to recognize an infinite conductivity vertical fracture flow regime and/or linear flow in an elongated reservoir. A partial penetration well (spherical flow) can be characterized by the negative one half slope pattern. The hump pattern is used to identify the transition period between wellbore storage and infinite acting radial flow regimes. A dual porosity behavior can be characterized by the dip pattern. Finally, a constant pressure boundary flow regime can be recognized by the steeply descending pattern at the end of the test.

Figure 3.3 shows a schematic diagram of the artificial neural network used in the study. There are ten processing units in the input layer, six units in the hidden layer, and eight units in the output layer. Each unit in the output layer represents a pattern. Since the behavior of any pattern has to be at least one log cycle long, the data used in the neural network training for all the patterns were one log cycle long. A log cycle of the training data consists of ten pressure derivative data points uniformly spaced in the logarithmic space since the pressure derivative curve is plotted on a logarithmic scale. We used the neural network to examine one log cycle of data (test cycle) at a time. By moving a "window" one log cycle wide from one point to the next in the actual well test, we could thereby identify the pattern for each point in the test.

The training data for all the patterns were randomly generated and normalized. A wide range of skins was used to generate the data for the hump pattern. A variety of transmissivity ratios (λ) in the dual porosity with pseudosteady state interporosity flow model was used to generated data for the dip pattern. A change in the value

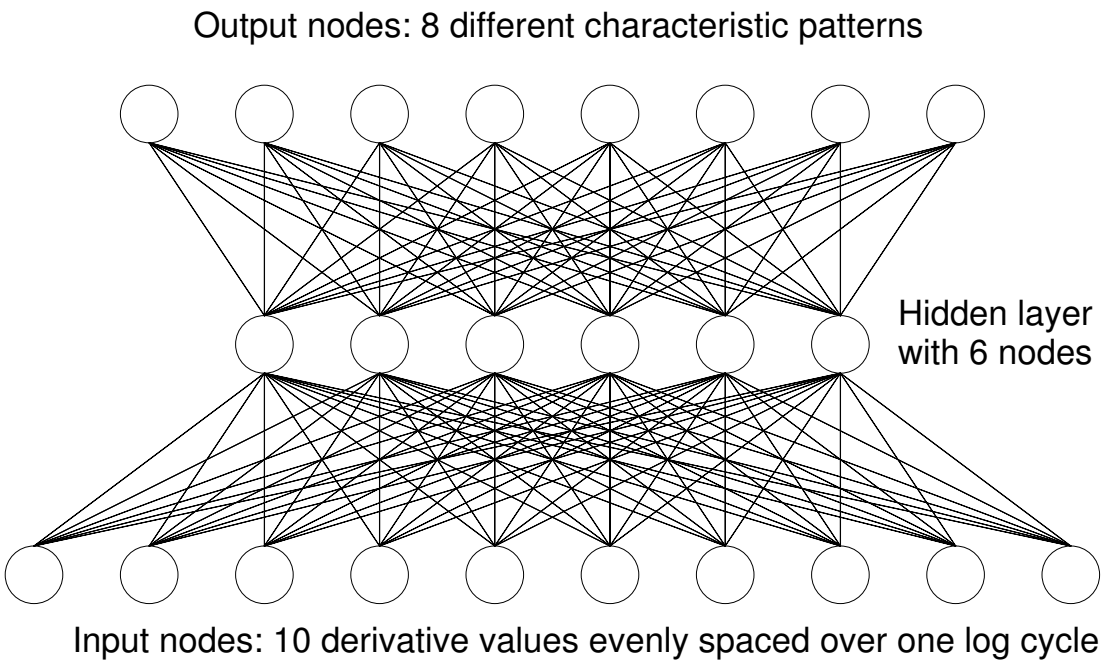

Figure 3.3: Schematic diagram of the artificial neural network used to characterize reservoir flow regimes

of storativity ratio (ω) does not affect the shape of the dip. It only shifts the dip pattern either to the left or to the right. Finally, different values of the distance to the boundary in the constant pressure boundary model were used to generate data in the descending pattern. The data for the rest of the patterns were generated from simple mathematical expressions yielding the desired slopes. A hundred sets of representative data for each pattern were used as the training data, and another one hundred sets of data for each pattern were used as the testing data. Figures 3.4 and 3.5 show the data used in the neural network training.

A program called *NevProp*, which was developed at the University of Nevada Center for Biomedical Modeling Research, was used to train the neural network in this study. *NevProp* is a general purpose back-propagation program written in C for UNIX, Macintosh, and DOS. The original version was *Quickprop* 1.0 by Scott Fahlman, as translated from Common Lisp into C by Terry Regier (1993). *NevProp* can be obtained via anonymous ftp to *unssun.scs.unr.edu* in the directory *pub/*

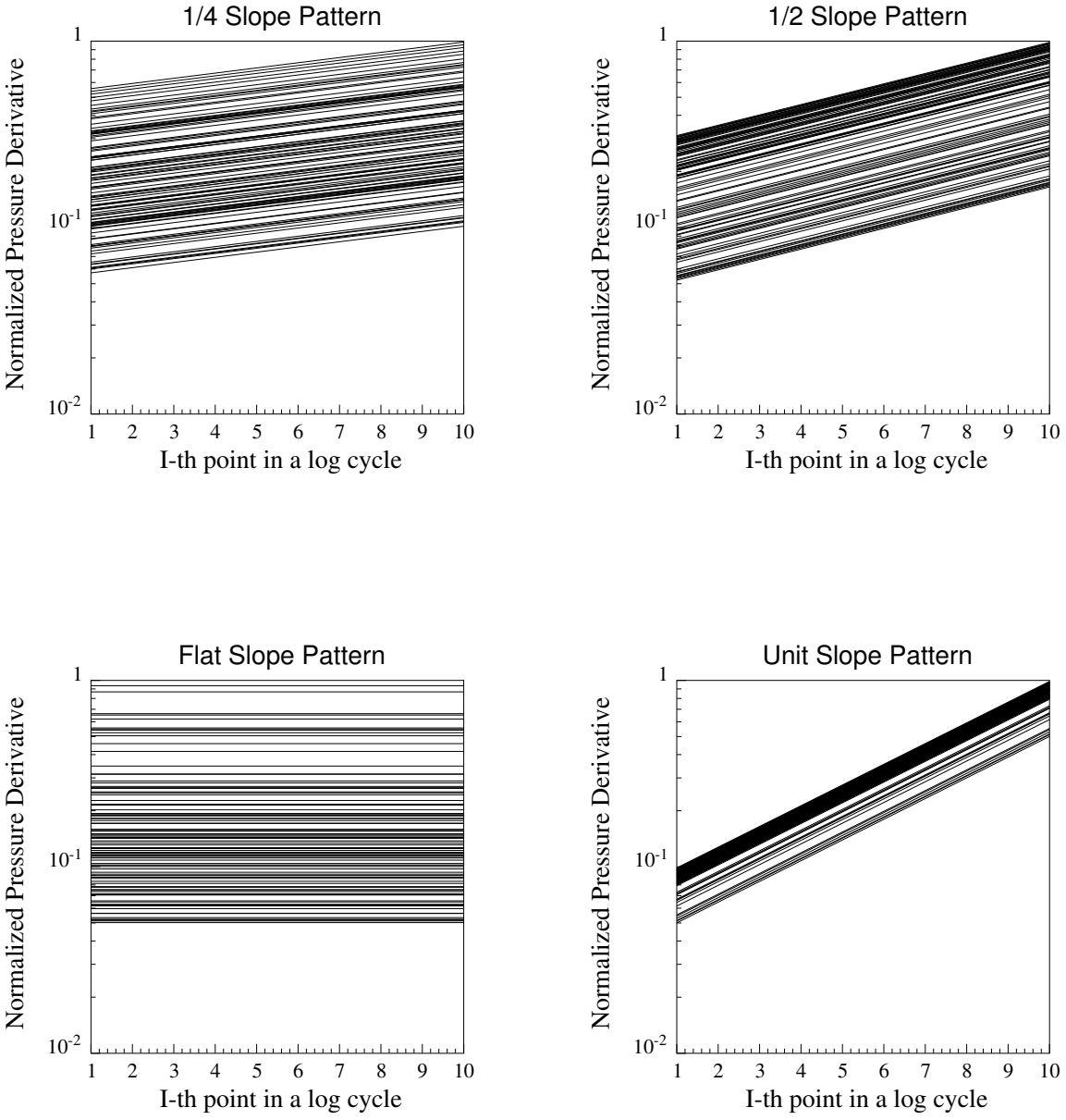

Figure 3.4: Training data used in the neural network training

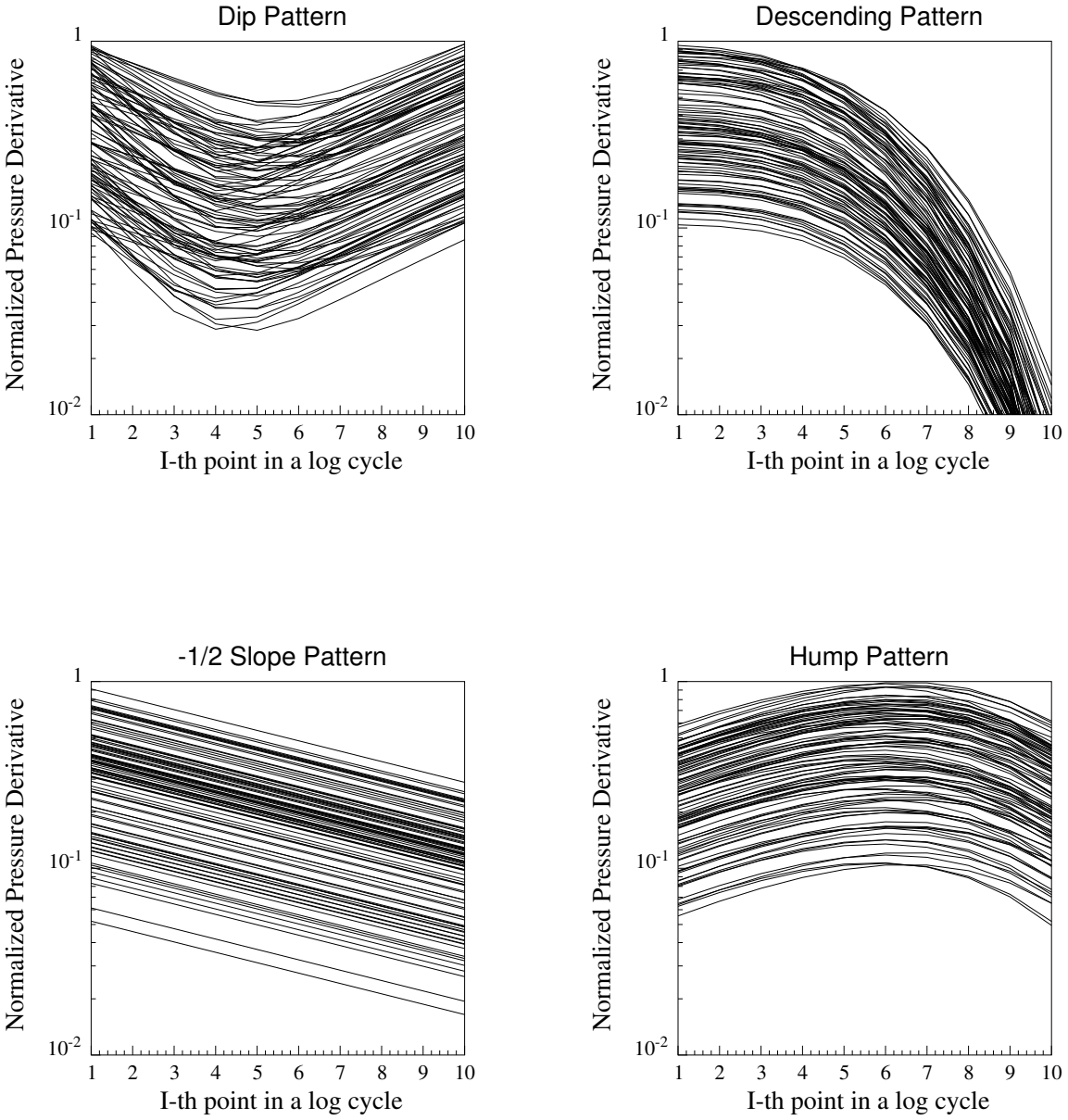

Figure 3.5: Training data used in the neural network training

goodman/ nevpropdir.

One of the crucial parameters in the neural network training is the number of processing units in the hidden layer which is typically related to the complexity of the problem. We had 10 input nodes (10 values of derivative) and 8 output nodes (8 characteristic patterns) in our neural network. Having tried several numbers of nodes in the hidden layer, we observed that the neural network with six hidden nodes yielded the most accurate results in the testing with real and simulated well test data. Our experience showed that a neural network with too many hidden units may excessively generalize the understanding of the training examples since it has a high degree of freedom (large number of weights). A neural network with more than six hidden nodes was able to identify the output of the training and testing data correctly more than 98 per cent of the time, however it also yielded intermediate or fairly high activation levels for other (incorrect) patterns as well. On the other hand, the training of a neural network with too few hidden nodes sometimes did not converge at all, even if converged the accuracy of the output prediction was generally low.

Neural network training usually consumes a lot of computer memory and CPU time. The level of consumption is related to the numbers of training and testing data, the numbers of processing units (first layer, hidden layer, and output layer), and the complexity of the problem. Characterizing eight different patterns using ten values of inputs is a relatively small task. In this study, the number of iterations in the training ranged from 2,000 to 30,000. The training was stopped when there was no more improvement over a large number of iterations (3000 or more). The network was then tested with well test data for its performance. Out of the many networks that were trained, a few of them were considered successful. However, these successfully trained neural networks still contained some weaknesses. A particular network was sometimes inferior in identifying a certain pattern or patterns. Great care should be taken in evaluating the neural network's accuracy in predicting reservoir flow regimes. This issue is discussed in Sections 4 and 5.

Although the neural network was trained to recognize all eight patterns mentioned before, the patterns of greatest interest are flat slope, unit slope, hump, dip, and descending slope. The purpose of this study was to investigate how the neural network

Table 3.2: Candidate reservoir models in the sequential predictive probability method

Model	Reservoir Model	Parameters
1	Infinite Acting	k, S, C
2	Sealing Fault	k, S, C, r_e
3	No Flow Outer Boundary	k, S, C, r_e
4	Constant Pressure Outer Boundary	k, S, C, r_e
5	Double Porosity with Pseudosteady State Interporosity Flow	k, S, C, ω, λ
6	Double Porosity with Pseudosteady State Interporosity Flow and Sealing Fault	k, S, C, ω, λ, r_e
7	Double Porosity with Pseudosteady State Interporosity Flow and No Flow Outer Boundary	k, S, C, ω, λ, r_e
8	Double Porosity with Pseudosteady State Interporosity Flow and Constant Pressure Outer Boundary	k, S, C, ω, λ, r_e

approach together with the sequential predictive probability method described by Anraku and Horne (1993) can be used to identify the reservoir model and its parameters. An existing program utilizing the sequential predictive probability method (Anraku 1993) discriminates between the eight reservoir models shown in Table 3.2. Being able to recognize the five patterns mentioned above, we can identify the flow regimes in all the eight models and hence make initial estimates of the reservoir parameters. Typical components of the pressure derivative curve for each reservoir model can be summarized in chronological order as follows:

1. Infinite acting radial flow:
    - unit slope, hump, flat slope.
2. Sealing fault boundary:
    - unit slope, hump, flat slope, transition, second flat slope (derivative doubles).

3. No flow outer boundary:
    - unit slope, hump, flat slope, unit slope.
4. Constant pressure outer boundary:
    - unit slope, hump, flat slope, descending pattern.
5. Dual porosity with pseudosteady state interporosity flow:
    - unit slope, hump, flat slope, dip, second flat slope or
    - unit slope, hump, dip, flat slope.
6. Dual porosity with pseudosteady state interporosity flow and sealing fault:
    - unit slope, hump, flat slope, dip, second flat slope, transition, third flat slope (derivative doubles).
    - unit slope, hump, dip, flat slope, transition, second flat slope (derivative doubles).
7. Dual porosity with pseudosteady state interporosity flow and no flow outer boundary:
    - unit slope, hump, flat slope, dip, second flat slope, unit slope or
    - unit slope, hump, dip, flat slope, unit slope.
8. Dual porosity with pseudosteady state interporosity flow and constant pressure outer boundary:
    - unit slope, hump, flat slope, dip, second flat slope, descending pattern or
    - unit slope, hump, dip, flat slope, descending pattern.

The initial estimates for reservoir parameters are computed using the pressure data in the appropriate flow regimes and then used as initial guesses for the estimation of reservoir parameters and the determination of reservoir model in the sequential predictive probability method. The procedure used in the evaluation of the initial estimates of reservoir parameters is described in the next section.

Section 4

Parameter Estimation and Model Identification

Since we do not intend to use the neural network as a model identification tool, all the eight reservoir models in Anraku's program were used as candidate models. The main purpose of the neural network is to identify reservoir flow regimes; hence, we can make initial estimates of reservoir parameters from the appropriate flow regimes. The sequential predictive probability method is very efficient in discriminating between reservoir models. Therefore, we used it for the model identification purpose.

The sequential predictive probability method described by Anraku and Horne (1993) requires initial estimates of reservoir parameters for all candidate reservoir models. Since we selected all the eight reservoir models as candidate models, we needed to make initial estimates for reservoir parameters for each of the models. This means that some flow regime parameters need to be estimated even if the flow regimes do not occur in the actual well test. For instance, the distance to a closed boundary needs to be estimated even if there is no unit slope found at the end of the test. This introduces a new complication to the approach since parameter estimates may need to be computed based on the location of a flow regime that is only inferred from other regimes found in the data.

This section discusses the procedures used to estimate the values of well storage coefficient, permeability, skin factor, distance to a closed boundary, distance to

a constant pressure boundary, distance to a fault boundary, storativity ratio, and transmissivity ratio. The procedure used to identify the reservoir flow regimes is then described. The basic procedure of the sequential predictive probability method is summarized at the end.

4.1 Wellbore Storage Coefficient

During the wellbore storage flow regime, the pressure change is a linear function of time. The plot of the pressure change versus time is a straight line. The value of wellbore storage coefficient(C) can be calculated using the following equation:

$$C = 0.0417\frac{qB}{\alpha} \tag{4.1}$$

where:

C = wellbore storage coefficient, STB/psi

q = production rate, STB/D

B = formation volume factor, $res\ vol/std\ vol$

α = slope from the plot of pressure change versus time, psi/hr

The wellbore storage flow regime can be identified by a presence of the unit slope pattern in the pressure derivative plot at the early time. If the neural network indicated that this flow regime exists, we then plotted the pressure change versus time for the log cycles that the wellbore storage lasts. The linear least squares approach was used to determine the best fitted straight line. Since the neural network is fairly tolerant to noise in the data, it was able to identify something close to a straight line, especially the very beginning of the hump pattern, as a unit slope straight line. Therefore, several straight lines were fitted for shorter ending times of the wellbore storage regime. The slope of the straight line with the lowest least squares error was used in Eqn. 4.1 to compute the wellbore storage coefficient.

In cases where the neural network did not identify the unit slope pattern at the early time, we started by plotting the pressure change against time for the entire first log cycle. Then, several plots with shorter wellbore storage regimes were made. The

slope used to calculate the wellbore storage coefficient was the slope of the straight line with the smallest least squares error.

4.2 Permeability and Skin

The values of permeability and skin can be estimated from the pressure data in the infinite acting period. In a drawdown test, a plot of the measured pressure versus a logarithm of time yields a straight line. The equation describing the straight line is written as follows:

$$p_{wf} = p_i - 162.6\frac{qB\mu}{kh}\left(log\ t + log\frac{k}{\phi\mu c_t r_w^2} + 0.8686S - 3.2274\right) \tag{4.2}$$

where:

p_{wf} = well flowing pressure, psi

p_i = initial reservoir pressure, psi

μ = viscosity, cp

k = permeability, md

h = thickness, ft

t = time, $hours$

ϕ = porosity, $dimensionless$

c_t = total system compressibility, psi^{-1}

r_w = wellbore radius, ft

S = skin factor, $dimensionless$.

Therefore, the value of permeability is calculated from the slope of the semilog plot as follows:

$$k = 162.6\frac{qB\mu}{mh} \tag{4.3}$$

where:

m = slope of the semilog plot, psi.

The value of skin can be estimated as follows:

$$S = 1.151\left(\frac{p_i - p_{1hr}}{m} - log\frac{k}{\phi\mu c_t r_w^2} + 3.2274\right) \tag{4.4}$$

where:

p_{1hr} = pressure at time 1 hour extrapolated from the fitted straight line, psi.

In a buildup test, a plot of the measured shut-in pressure versus a logarithm of Horner time yields a straight line. The equation describing the straight line is written as:

$$p_{ws}(\Delta t) = p_i - 162.6\frac{qB\mu}{kh}\ log\left(\frac{t_p + \Delta t}{\Delta t}\right) \tag{4.5}$$

where:

p_{ws} = shutin pressure, psi

t_p = producing time, $hours$

$\frac{t_p+\Delta t}{\Delta t}$ = Horner's time, $dimensionless$

The flat derivative curve in the infinite acting period can be recognized as the flat slope pattern by the neural network. The data in the log cycles that were identified as belonging to the flat slope pattern were plotted versus the logarithm of time or Horner time depending on the type of the test. The best fitted straight line was determined by performing the linear least squares fit. As previously mentioned, the neural network is fairly tolerant to noise. Therefore, several plots were generated with different starting and ending points for the infinite acting period. The starting point was shifted forward in each plot since the neural network sometimes recognized the pressure derivative curve as being flat before it actually becomes flat. The ending point was shifted backward in each plot because the neural network may identify the beginning of the flow regime after the end of the infinite acting period as infinite acting. The most likely infinite acting radial flow period was determined from the straight line whose linear least squares error is the minimum.

Since the neural network trained in this study sometimes misclassified the peak of a hump as flat, we found it necessary to be very careful in identifying the true infinite acting period. From principles of well test interpretation, we know that the infinite acting flow regime typically occurs about one and a half log cycles after the

end of wellbore storage. Therefore, any flat region that occurs before this period needs to be discarded. In some cases, the neural network did not identify any flat regions at all. This generally happened when the flat zone was shorter than a log cycle or the data were too noisy. In this case, we assumed that the infinite acting period starts at a time one and a half log cycles away from the end of the wellbore storage and lasts for a log cycle (or less if the test is terminated before a log cycle of data are obtained). The selected data were fitted by a semilog straight line. Then, several semilog straight lines were fitted with different starting and ending points for the infinite acting period. The semilog straight line with the minimum least squares error was chosen to compute the values of permeability and skin.

4.3 Distance to Closed Boundary

The distance to a closed boundary can be estimated from the pressure data in the pseudosteady state flow period. During this period, the pressure change is a linear function of time as described by the following equation:

$$p_i - p_{wf} = \frac{0.2342\ qB}{\phi c_t h A}\ t\ +\ 70.65\frac{qB\mu}{kh}\left(ln\left(2.2458AC_A r_w^2\right)\ +\ 2S\right) \tag{4.6}$$

where:

A = reservoir area, ft^2

C_A = shape factor, $dimensionless$

A Cartesian plot of pressure change versus time yields a straight line. The area of the reservoir can be calculated as follows:

$$A = \frac{0.2342\ qB}{\phi c_t h\ m_{Cartesian}} \tag{4.7}$$

where:

$m_{Cartesian}$ = slope of the Cartesian plot, psi/hr.

The distance to the boundary (r_e) in a circular reservoir is calculated as follows:

$$r_e = \sqrt{\frac{A}{\pi}} \tag{4.8}$$

In a drawdown test, the pseudosteady flow shows up as a unit slope at late time in the derivative plot. The pressure drops in the log cycles that were classified by the neural network as having a unit slope were plotted against time. The linear least squares method was used to fit the best straight line. Several plots were generated with different starting times of the pseudosteady state regime. The straight line with the minimum least squares error was used in the computation of the distance to the boundary.

The neural network may not identify the data as belonging to the unit slope pattern at the time. This was found to happen in three cases as follows:

1. There is actually no unit slope if the test has been terminated before it reaches the closed boundary or if there is another kind of boundary (constant pressure or fault boundary). As mentioned earlier, we have to supply initial estimates for all of the model parameters to the sequential predictive probability procedure so that it can perform model discrimination. Therefore, we need to estimate the distance to a potential closed boundary even when none is evident. If there was no sign of other kind of boundary, we used the radius of investigation at the end of the test as the distance to the closed boundary. If there exists other kinds of boundary, we used the distance to that boundary as an initial guess for the distance to the closed boundary.

2. The closed boundary actually exists but the unit slope region from the test is shorter than a log cycle. In this case, we estimated roughly that the boundary is reached when the test is terminated. Therefore, we used the radius of investigation at the end of the test as the distance to the closed boundary.

3. The closed boundary actually exists but the unit slope region is too noisy to be recognized. In this case, we also estimated roughly that the boundary is reached when the test is terminated. Therefore, we used the radius of investigation at the end of the test as the distance to the closed boundary.

Recall that these initial estimates are just preliminary guesses to be used in the sequential predictive probability method. The radius of investigation is a fairly reasonable guess for the distance to the boundary. The radius of investigation (r_{inv}) can

be computed as Lee (1982) described as follows:

$$r_{inv} = \sqrt{\frac{4 \times 0.0002637kt}{\phi \mu c_t r_w^2}} \tag{4.9}$$

In a buildup test, the pressure derivative decreases when the pressure transient approaches the boundary of any kind. Therefore, the distance to any kind of boundary can be estimated by the radius of investigation at the time when the pressure derivative starts to decrease or at the end of the test if the boundary has not been reached.

4.4 Distance to Constant Pressure Boundary

When the pressure transient reaches a constant pressure boundary, the reservoir encounters a steady state flow regime. The pressure at the well becomes constant and can be expressed in terms of dimensionless pressure drop (p_D) as follows:

$$p_D = ln\ \frac{r_e}{r_w} \tag{4.10}$$

The dimensionless pressure drop also includes the skin. Substituting the definition of p_D back into Eqn. 4.10, we obtain:

$$\frac{kh}{141.2\ qB\mu}(p_i - p_{wf}) + S = \ ln\ \frac{r_e}{r_w} \tag{4.11}$$

Therefore, the distance to the constant pressure boundary can be calculated as follows:

$$r_e = r_w\ e^{\frac{kh}{141.2\ qB\mu}(p_i - p_{wf}) + S} \tag{4.12}$$

The pressure derivative decreases and reaches zero when the flow regime approaches the steady state regime. We used the neural network to recognize this regime as the descending pattern. The only unknown in Eqn. 4.12 is the pressure drop $(p_i - p_{wf})$. The pressure data that were identified as belonging to the descending pattern at the end of the test were used to compute the distance to the constant

pressure boundary. In most cases, the pressure derivatives were too noisy to be recognized or sometimes became negative even if there were minor errors in the pressure measurement. Therefore, the pressure derivative may not necessarily have a descending pattern. In this case, we checked if the pressure drop for the last half log cycle was relatively constant. If it was, we assumed that the reservoir had encountered the steady state regime, and the distance to the boundary was evaluated using the average value of the relatively constant pressure.

If the descending pattern of the derivative was not noticed by the neural network and if the pressure drops were not constant, we used the radius of investigation at the end of the test as a guess for the distance to the constant pressure boundary.

In a buildup test, we see a descending pattern when the test reaches any kind of boundary. Therefore, we used the radius of investigation at the time the pressure derivative starts to descend as a guess for the distance to the constant pressure boundary. If the neural network signals did not indicate a presence of the descending pattern, the radius of investigation at the end of the test was used instead.

4.5 Distance to Fault Boundary

A presence of a fault boundary can be detected by the doubling in slope of the semilog plot. The distance to the fault boundary (d) can be computed using the time the first straight line meets with the second straight line as Davis and Hawkins (1963) and Gray (1965) described as follows:

$$d = \sqrt{\frac{1.48 \times 10^{-4}\ k\ t_x}{\phi \mu c_t}} \tag{4.13}$$

where:

t_x = time at which the two straight lines intersect, hr.

In a drawdown test, the pressure derivative is flat for the period of the first semilog straight straight line, then transitionally increases, and becomes flat again during the period of the second semilog straight line. The value of the pressure derivative of the second flat region is twice that of the first flat region. These two flat regions could be recognized by the neural network on the condition that the flat regions have to

be apart with a transition in between and the average value of the second pressure derivative has to be about twice that of the first flat region. After recognizing the two regions, several semilog plots were created with different starting and ending times for both flat regions. The semilog straight line with the minimum least squares error was chosen for each region. The intersection of the two best straight lines was then determined and used to calculate the distance to the fault boundary.

If the neural network did not identify that there were two separate flat regions, the radius of investigation at the end of the test was then used as an initial guess for the distance to the fault boundary in the sequential predictive probability method.

In a buildup test where we cannot distinguish the type of boundary being encountered, we used the radius of investigation as an initial guess for the distance to the fault boundary.

4.6 Storativity Ratio and Transmissivity Ratio

A presence of a dip in the derivative curve suggests that the reservoir is heterogeneous. The dual porosity parameters (ω and λ) can be determined from the minimum point of the dip using a procedure described by Bourdet, Whittle, Douglas, Pirard and Kniazeff (1983b). At the minimum point,

$$t_D p_D\prime = \frac{1}{2}\left(1 + \omega^{\frac{1}{1-\omega}} - \omega^{\frac{\omega}{1-\omega}}\right) \tag{4.14}$$

and

$$t_D = \frac{\omega}{\lambda}\, ln\, \frac{1}{\omega} \tag{4.15}$$

Since the relationship between the storativity ratio (ω) and the pressure derivative ($t_D p_D\prime$) is nonlinear, we applied the Newton-Raphson procedure to calculate the value of ω at a given value of pressure derivative (the value at the minimum point). Figure 4.1 shows the log-log plot of the storativity ratio and the pressure derivative as well as a simple log-log straight line fitted to the curve. This fitted straight line was used to estimate an initial value of the storativity ratio in the Newton-Raphson procedure and is described by the following equation:

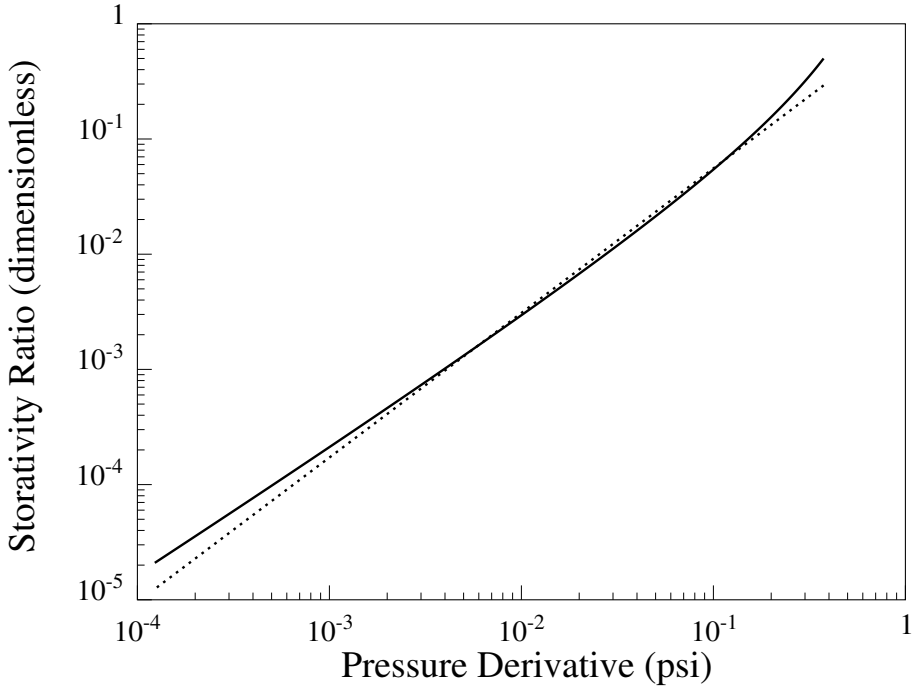

Figure 4.1: Storativity ratio (ω) as a function of pressure derivative ($t_D\ p_D\prime$) and the fitted log-log straight line.

$$\omega = (t_D p_D\prime)^{1.255} \tag{4.16}$$

Applying the Newton-Raphson procedure, the value of ω can be calculated as follows:

$$\omega_{new} = \omega_{old} - \frac{f(\omega_{old})}{f\prime(\omega_{old})} \tag{4.17}$$

where

$$f(\omega) = 1 + \omega^{\frac{1}{1-\omega}} - \omega^{\frac{\omega}{1-\omega}} - 2\ t_D p_D\prime \tag{4.18}$$

and

$$f\prime(\omega) = \frac{ln\ \omega}{(1-\omega)^2}\left(\omega^{\frac{1}{1-\omega}} - \omega^{\frac{\omega}{1-\omega}}\right) \tag{4.19}$$

We performed the Newton-Raphson iteration until the absolute difference between ω_{old} and ω_{new} became smaller than some preset tolerance. After obtaining the estimate for ω, the estimate of λ can be determined as follows:

$$\lambda = \frac{\omega}{t_D}\, ln\, \frac{1}{\omega} \tag{4.20}$$

The neural network was used to identify the presence of the dip pattern. The minimum point of the dip pattern was determined by comparing the values of the pressure derivative in the vicinity of the dip pattern. If the dip pattern did not exist or was not identified by the neural network, an initial guess of 0.99 was used for both ω and λ.

4.7 Step by Step Procedure in Identifying Reservoir Flow Regimes

This part describes the procedure used to identify the reservoir flow regimes from the neural network's signals so that the reservoir parameters can be evaluated as previously described. For a drawdown test, the procedure can be summarized as follows:

1. Look for the unit slope pattern.
    - Unit slope region at early times exists (activation level greater than 0.8).
        - Use the data in the identified log cycles to calculate the wellbore storage coefficient. Then, experiment with shorter periods of wellbore storage.
    - Unit slope region at early times does not exist.
        - Use the data in the first log cycle to calculate the wellbore storage coefficient. Experiment with shorter periods of wellbore storage.
    - Unit slope region at late times exists (activation level greater than 0.8).

  - Use the data in the identified log cycles to calculate the distance to the closed boundary. Experiment with later starting times for the unit slope region.

- Unit slope region at late times does not exist.
  - If another kind of boundary is detected, use the distance to that boundary as a guess for the distance to the closed boundary.
  - If another kind of boundary is not detected, use the radius of investigation at the end of the test as a guess for the distance to the closed boundary.

2. Look for the hump pattern (activation level greater than 0.8).
   - Late time hump is discarded.

3. Look for the flat slope pattern.

   - Flat slope region exists (activation level greater than 0.8).
     - If the flat slope region is about one and a half log cycles after the last point in the early time unit slope or the beginning of the early time hump, use the data in the identified log cycles to compute permeability and skin. Experiment with different starting and ending times. Use the radius of investigation or the distance to other kinds of boundary as a guess for the distance to the fault boundary if no other flat region is detected.
     - If the flat slope region is less than one and a half log cycles after the last point in the early time unit slope or the beginning of the early time hump, discard that flat slope and look for another one. If none exists, proceed as if the flat slope did not exist.
     - If the flat slope region exists but the early time unit slope and the early time hump do not exist, use the identified log cycles of the flat slope to compute the permeability and skin. Experiment with different starting and ending times. Use the radius of investigation or the distance

to other kinds of boundary as a guess for the distance to the fault boundary if no other flat region is detected.

  - If the flat slope region starts more than two and a half log cycles after the last point in the early time unit slope or the beginning of the early time hump, there is a chance that the fault boundary exists. Use a log cycle of data that is one and a half log cycles after the last point in the early time unit slope or the beginning of the early time hump to compute the permeability, skin, and slope of the semilog straight line. Then, use the identified log cycles of the flat slope region to compute the slope of the second semilog straight line. If the slope of the second semilog straight line is twice that of the first one, then compute the distance to the fault boundary. If not, use the radius of investigation or the distance to other kinds of boundary as a guess for the distance to the fault boundary. Experiment with different starting and ending times for both semilog straight lines.
  - If two flat slope regions exist and they are at least half a log cycle apart, there is a chance that the fault boundary exists. Use the identified log cycles of the first flat region to compute the permeability, skin, and slope of the first semilog straight line. Then, use the identified log cycles of the second flat slope region to compute the slope of the second semilog straight. If the slope of the second semilog straight line is twice that of the first one, then compute the distance to the fault boundary. If not, use the radius of investigation or the distance to other kinds of boundary as a guess for the distance to the fault boundary. Experiment with different starting and ending times for both semilog straight lines.

- Flat slope region does not exist.
  - If the early time unit slope region and/or the early time hump region exist, use a log cycle of data that is one and a half log cycles after the last point in the early time unit slope or the beginning of the early time hump to compute the permeability and skin. Experiment with

different starting and ending times. Use the radius of investigation or the distance to other kinds of boundary as a guess for the distance to the fault boundary.

- If neither the early time unit slope nor early time hump patterns exist, the method fails to recognize the infinite acting period.

4. Look for the dip pattern.

   - Dip region exists (activation level greater than 0.8).
     - Determine the minimum point of the dip and use it to compute the values of storativity and transmissivity.
   - Dip region does not exist.
     - Use 0.99 as guesses for both values of storativity and transmissivity.

5. Look for the constant pressure at the end of the test.

   - Pressure stays constant for the last half log cycle.
     - Use the data in the last half log cycle to compute the distance to the constant pressure boundary.
   - Pressure does not stay constant for the last half log cycle.
     - If another kind of boundary is detected, use the distance to that boundary as a guess for the distance to the constant pressure boundary.
     - If another kind of boundary is not detected, use the radius of investigation at the end of the test as a guess for the distance to the constant pressure boundary.

For a buildup test, the above procedure still applies for the wellbore storage and infinite acting flow regimes. The only change is the recognition of the flow regime when the test approaches a boundary. The radius of investigation at the time when the derivative starts to decrease or at the end of the west is used as initial guesses for the distance to the closed boundary, the distance to the fault boundary, and the distance to the constant pressure boundary.

4.8 Model Identification by Sequential Predictive Probability Method

The basic procedure of the sequential predictive probability method for model discrimination in well test analysis was summarized by Anraku and Horne (1993) as follows:

1. Select several candidate reservoir models which might be consistent with both the pressure data and other available information.

2. Use the first several pressure data points to estimate the reservoir parameters and predict the probability distribution of the pressure at the next time point under each of the reservoir models.

3. Calculate the probability by substituting the actual pressure data at the next time point into the predictive probability distribution under each reservoir model and update the joint probability under each reservoir model be multiplying the joint probability by the probability.

4. Repeat this procedure until a difference of the joint probability between reservoir models is obtained.

5. Discrimination between candidate reservoir models is performed according to this joint probability.

In our approach, we used all the eight available reservoir models in the sequential predictive probability program as candidate reservoir models.

Section 5

Results and Discussion

This section discusses the results obtained by combining the artificial neural network and the sequential predictive probability methods. Three sets of actual field data and three simulated tests with random noises are discussed. In each example, the artificial neural network program was used to identify different reservoir flow regimes. Then, initial estimates of reservoir parameters were made and used as initial guesses in the sequential predictive probability program.

Since the spacing of the data used to train the neural network are uniform in the logarithmic sense, the spacing of the pressure derivatives whose pattern is to be characterized by the neural network needs to be logarithmically uniform as well. Ten data points are needed for each log cycle in the neural network program. These ten values of pressure derivatives were linearly interpolated between adjacent points at the desired spacing. The pressure derivatives are generally nonlinear, but we have no other information on how the pressure derivative curve can be described in mathematical terms in order to perform the most appropriate interpolation scheme. In fact, this is what we wanted to determine. By the nature of the well test, the linear interpolation scheme seems to be suitable. At very early times when there is a relatively small number of measurements, the response is typically still in the wellbore storage flow regime. The pressure derivative in this flow regime is a linear function of time. Therefore, the linear interpolation scheme applies here. At larger time values, there are usually plenty of data points in a log cycle since the pressure is measured

at relatively small time intervals and plotted on a logarithmic scale. Therefore, the linear interpolation method does not distort the shape of the pressure derivatives. In cases where there is a permanent downhole pressure gauge, we generally do not see the presence of wellbore storage, but the downhole pressure gauge usually records the data continuously at very small time intervals. Therefore, the linear interpolation scheme still applies in this case. In any case, one of the reasons we used the neural network approach to characterize the flow regime is that it is tolerant to noise. Therefore, smoothing the data is not a necessary nor even a desirable procedure.

5.1 Application to Actual Field Test Data

We experimented with a number of sets of real and simulated well test data to evaluate the effectiveness of the approach. Three sets of actual field data with different shapes of pressure derivative curve were selected to illustrate the behavior of the method.

5.1.1 Test 1: Damaged Well

The data for this buildup test were obtained from Test 8 in the book by Horne (1995). Table 5.1 shows the values of the well and reservoir parameters. The pressure data are shown in Table 5.2. The well was shut in for approximately 11 hours after it had been on production for about 204 hours. The pressure derivatives are plotted in Figure 5.1 both in the original and in the interpolated uniform spacings. The pressure derivative plot clearly shows the wellbore storage flow regime, transition period, and infinite acting radial flow regime in a chronological sequence.

Shown under the two derivative plots in Figure 5.1 are the activation levels from the neural network program for four patterns: unit slope, flat slope, hump, and dip. The activation level of the unit slope pattern is approximately 1 for the first few log cycles of data. Then, about half a log cycle later, the activation level of the hump pattern becomes approximately 1. At the same time, the flat slope pattern becomes activated with an activation value of 0.5. This point is actually the peak of the hump. The neural network was not sure whether the input belongs to the flat slope pattern.

Table 5.1: Well and reservoir parameters for Test 1

Parameter	Value
Type of test	Buildup
Wellbore radius	0.35 ft
Porosity	0.28
Formation thickness	100 ft
Flow rate	1812 bbl/day
Viscosity	0.6 cp
Formation volume factor	1.25 bbl/STB
Total compressibility	12.0×10^{-6} psi^{-1}
Initial pressure	2218.46 psia
Producing time	204.47 hr

In this study, any activation level less than 0.8 was not considered as an identification of a pattern. The activation level of the dip pattern jumps to 0.4 when the derivatives have a half-valley shape. Again, this pattern was not accounted for because of the low activation level.

The neural network identification of the presence of the unit slope and the hump agrees with our previous human observation. However, the neural network did not identify the flat region at the infinite acting flow regime. This is because the data in the flat region are too short to be recognized. If we as human observer were asked to identify the pattern of the last ten data points solely without looking at the previous behavior of the derivatives, we may not identify it as a flat slope pattern. From principles of well test analysis, we know that the infinite acting radial behavior typically occurs about one and a half log cycles after the end of the wellbore storage flow regime. Possessing this reasoning ability, we can then identify this last part of the derivative curve as a flat region. The neural network does not contain this knowledge. Therefore, we need to incorporate our knowledge of well testing into the algorithm that interprets the signals from the neural network. In cases where there was no flat slope signal from the neural network, about a log cycle of data points that lie approximately one and a half log cycles after the end of the storage were considered to represent the infinite acting radial flow regime.

Table 5.2: Well test data for Test 1

Time (hours)	Pressure (psia)	Time (hours)	Pressure (psia)	Time (hours)	Pressure (psia)
204.4875	1815.3697	205.8000	2176.5597	210.8000	2192.0897
204.4903	1824.3597	205.9667	2177.9797	210.9667	2192.3097
204.4931	1831.2597	206.1333	2179.3297	211.1333	2192.4697
204.4958	1837.1797	206.3000	2180.3097	211.3000	2192.7597
204.5000	1848.0597	206.4667	2181.2397	211.4667	2192.9000
204.5083	1866.7597	206.6333	2182.0197	211.6333	2193.1000
204.5139	1878.8197	206.8000	2182.8897	211.8000	2193.2897
204.5250	1902.6797	206.9667	2183.6000	211.9667	2193.4397
204.5417	1936.9000	207.1333	2184.2397	212.1333	2193.6097
204.5583	1967.1197	207.3000	2184.6697	212.3000	2193.8097
204.5750	1994.9197	207.4667	2185.3197	212.4667	2193.9797
204.5917	2020.1597	207.6333	2185.7197	212.6333	2194.1497
204.6083	2041.7397	207.8000	2186.1497	212.8000	2194.3097
204.6250	2061.0797	207.9667	2186.4897	212.9667	2194.4897
204.6417	2077.4597	208.1333	2186.8497	213.1333	2194.6000
204.6583	2091.3000	208.3000	2187.1297	213.3000	2194.8197
204.6750	2103.1897	208.4667	2187.5097	213.4667	2195.0000
204.7000	2117.5097	208.6333	2187.9000	213.6333	2195.0797
204.7333	2131.6897	208.8000	2188.2297	213.8000	2195.1897
204.7657	2141.1797	208.9667	2188.5597	213.9667	2195.4097
204.8000	2147.9697	209.1333	2189.4897	214.1933	2195.5097
204.8667	2156.1597	209.3000	2189.9697	214.3000	2195.6797
204.9333	2160.8797	209.4667	2190.2597	214.4667	2195.7797
205.0500	2165.7000	209.6333	2190.5897	214.6333	2195.9097
205.1000	2167.0000	209.8000	2190.7897	214.8000	2196.1197
205.1667	2168.4397	209.9667	2191.0197	214.9667	2196.1000
205.2333	2169.8697	210.1333	2191.2897	215.1333	2196.2000
205.3000	2171.0197	210.3000	2191.5697	215.3000	2196.3000
205.4667	2173.4397	210.4667	2191.6197	215.4667	2196.4597
205.6333	2175.0897	210.6333	2191.8897	215.6333	2196.6197

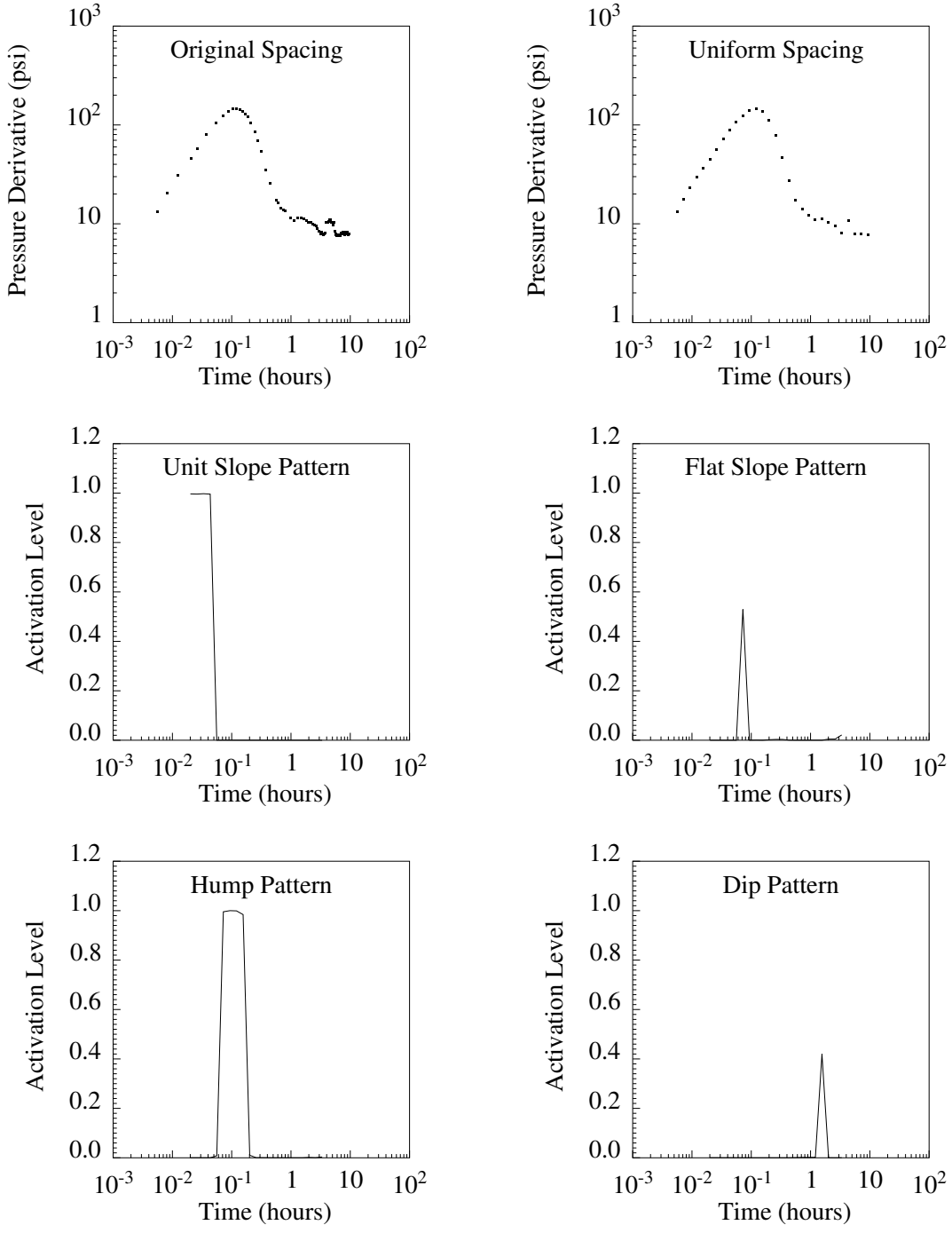

Figure 5.1: Activation levels of different patterns from neural network for Test 1

Table 5.3: Initial estimates of reservoir parameters for Test 1

Parameter	Initial Estimate
k	117.30
S	15.78
C	0.041
ω	0.99
λ	0.99
r_e	827.07

After identifying the reservoir flow regimes, we were then able to make initial estimates of reservoir parameters from the relevant data. Table 5.3 shows the initial estimates of reservoir parameters obtained by using the procedures described in Section 4.

The sequential predictive probability program was then run using all the eight reservoir models as candidate models and the computed estimates as initial guesses for reservoir parameters. The output from the program consists of normalized joint probabilities, eventual estimates of reservoir parameters, and confidence intervals. The normalized joint probability is a measure of the likelihood that the reservoir can be described by a particular model. The normalized joint probabilities of significant values for this test are plotted as a function of time in Figure 5.2. The infinite acting reservoir model has the highest normalized joint probability at the end of the test; hence, the reservoir is most likely in the infinite acting flow regime. Shown above the normalized probability plot is the derivative plot depicting the fitted curves generated from the infinite acting radial flow model.

The initial estimates from the neural network program and the eventual estimates from the sequential predictive probability program are compared in Table 5.4. The initial estimates are reasonably close to the eventual values of the reservoir parameters. Hence, the neural network and its associated parameter estimation algorithm have been found to be effective in obtaining good initial estimates for the parameter values. The confidence intervals for all the parameters are also summarized in Table 5.4. Generally, confidence intervals may be viewed as tools in verifying the

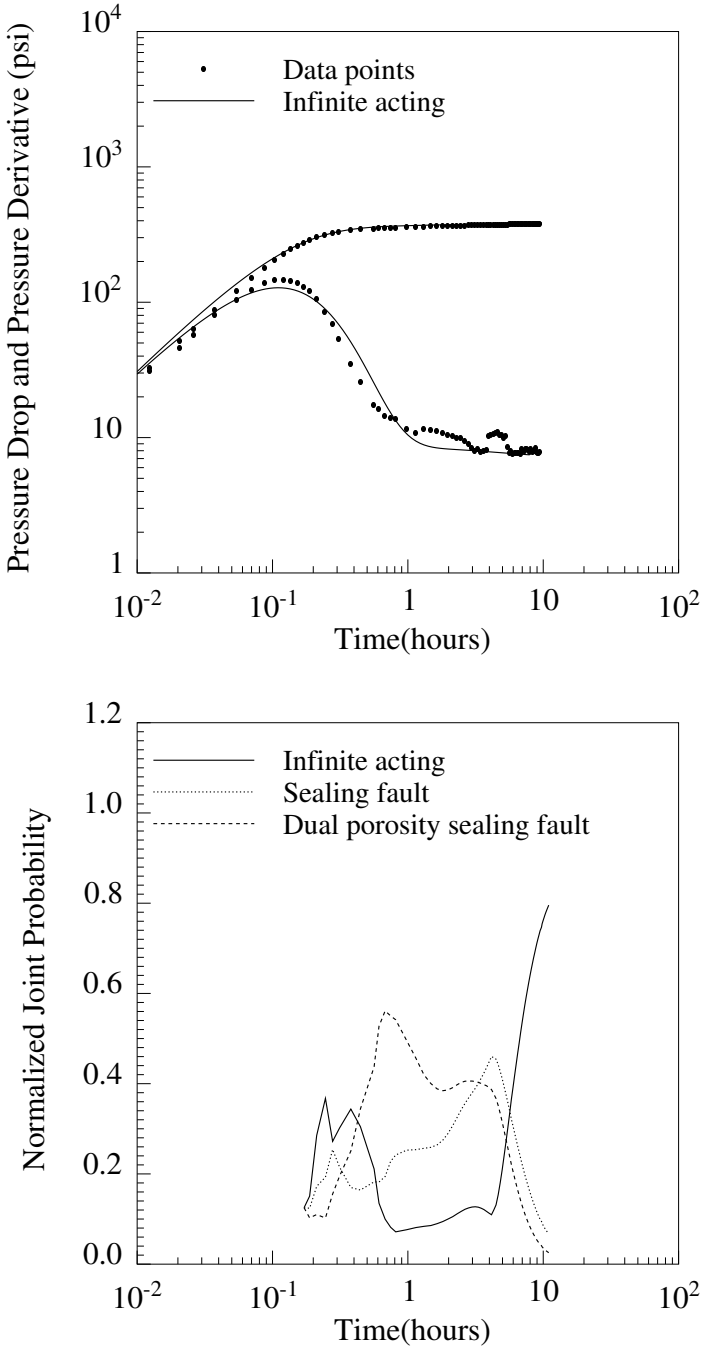

Figure 5.2: Matches to the data points (upper) and the corresponding normalized joint probability (lower) for Test 1

Table 5.4: Comparison between the initial estimates and fitted values of reservoir parameters for Test 1

Parameter	Initial Estimate	Eventual Estimate	Confidence Interval
k	117.30	128.12	$\pm$ 1.72%
S	15.78	18.37	$\pm$ 0.054
C	0.041	0.029	$\pm$ 2.26%

selected reservoir model. In our case, the normalized probability from the sequential predictive probability approach itself is a better tool to validate the reservoir model. The confidence intervals are shown here as a subsidiary verification.

5.1.2 Test 2: Stimulated Well

The test data for this buildup test were taken from Test 1 in the book by Horne (1995). Table 5.5 shows the values of the well and reservoir parameters. The pressure data are shown in Table 5.6. This well was shut in for about 188 hours after it had been on production for more than a year. Since the production time is long and unknown, the test was treated as a drawdown test with a negative flow rate (see Test 1 in Horne, 1995). The pressure derivatives and the activation levels for different characteristic patterns in the neural network are plotted in Figure 5.3.

The unit slope pattern (wellbore storage) is present for the first few log cycles of the data and followed by the hump pattern together with the flat slope pattern. This flat slope pattern is not actually the infinite acting radial flow regime since it happens too close to the end of the wellbore storage. The true infinite acting region is about one and a half log cycles after the end of the wellbore storage regime, which the neural network did not characterize as a flat slope region. However, we could determine the infinite acting radial flow using the earlier argument; hence, the values of permeability and skin could be calculated. After characterizing all the flow regimes, the initial estimates of the reservoir parameters required by the eight reservoir models were estimated. They are summarized in Table 5.7.

After running the sequential predictive probability program with the computed

Table 5.5: Well and reservoir parameters for Test 2

Parameter	Value
Type of test	Buildup
Wellbore radius	0.30 ft
Porosity	0.20
Formation thickness	100 ft
Flow rate	500 bbl/day
Viscosity	0.548 cp
Formation volume factor	1.315 bbl/STB
Total compressibility	15.94×10^{-6} psi^{-1}
Initial pressure	2615.08 psia

Table 5.6: Well test data for Test 2

Time (hours)	Pressure (psia)	Time (hours)	Pressure (psia)	Time (hours)	Pressure (psia)
0.0011	2616.3100	19.7366	2680.1600	142.2632	2718.6500
0.0910	2616.6000	21.7526	2682.3900	154.3713	2720.1700
0.2926	2617.9600	23.7686	2684.3400	160.5873	2721.2200
1.1670	2624.7400	27.2966	2687.6100	162.6033	2720.8800
2.1750	2631.7700	31.3286	2690.7300	164.6193	2721.2200
3.1830	2638.0000	35.3606	2693.2700	166.0347	2721.4200
4.1910	2643.3300	40.9170	2696.5400	167.0427	2721.4900
5.1990	2647.8100	46.9650	2698.6800	168.0507	2721.6700
6.2070	2651.6300	53.0130	2700.9700	169.0587	2721.6500
7.2150	2654.8900	59.0610	2702.9300	181.4946	2722.5700
8.2230	2657.9500	65.1510	2705.0100	182.5026	2722.7400
9.2310	2660.7500	71.2012	2706.1100	183.5106	2722.9200
10.2390	2663.4300	77.2492	2707.8400	184.5186	2723.1300
11.2470	2665.8200	83.2972	2709.4200	185.5266	2723.1800
12.2550	2668.0000	89.3433	2711.1300	186.5346	2723.3200
13.2630	2670.1200	95.3912	2711.8600	187.5426	2723.2600
14.2710	2672.1600	105.9752	2713.7400	188.5506	2723.3200
15.5366	2674.4000	118.0712	2715.5300	188.7186	2723.2800
17.7206	2677.7300	130.1672	2717.1700		

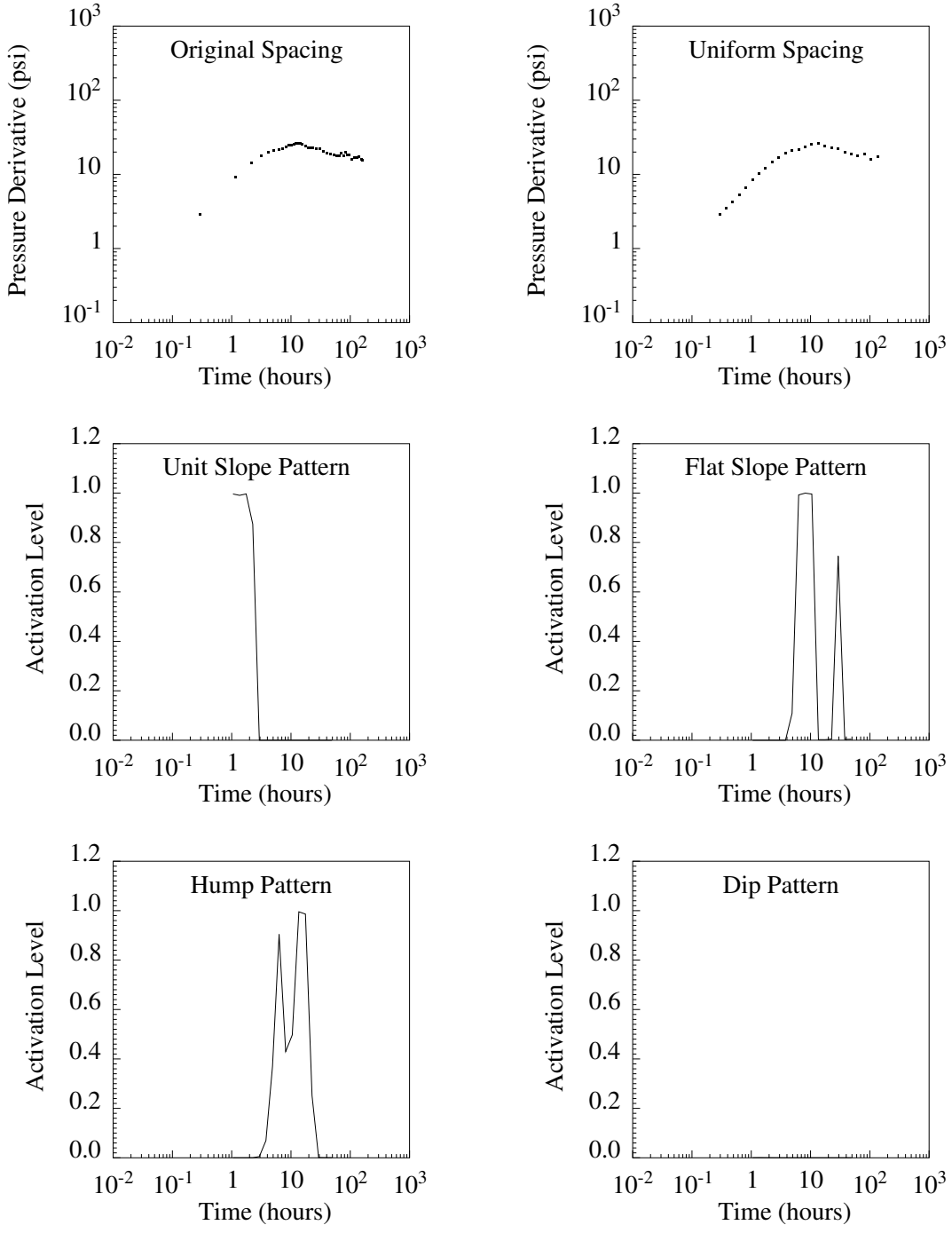

Figure 5.3: Activation levels of different patterns from neural network for Test 2

Table 5.7: Initial estimates of reservoir parameters for Test 2

Parameter	Initial Estimate
k	13.34
S	-5.14
C	4.21
ω	0.99
λ	0.99
r_e	1232.49

Table 5.8: Comparison between the initial estimates and fitted values of reservoir parameters for Test 2

Parameter	Initial Estimate	Eventual Estimate	Confidence Interval
k	13.34	17.52	$\pm$ 2.55%
S	-5.14	-4.39	$\pm$ 0.686
C	4.21	2.51	$\pm$ 2.57%

initial estimates, the normalized joint probabilities of significant values are plotted in Figure 5.4. The infinite acting model has the highest normalized joint probability at the end of the test, and hence the most likely reservoir model. Shown above the normalized joint probability plot is the original pressure derivative with the fitted infinite acting radial flow curves. The initial estimates from the neural network program, the eventual estimates from the sequential predictive probability program, and the confidence intervals for all the parameters are summarized in Table 5.8. The initial estimates were found to be relatively close to the eventual estimates of the reservoir parameters.

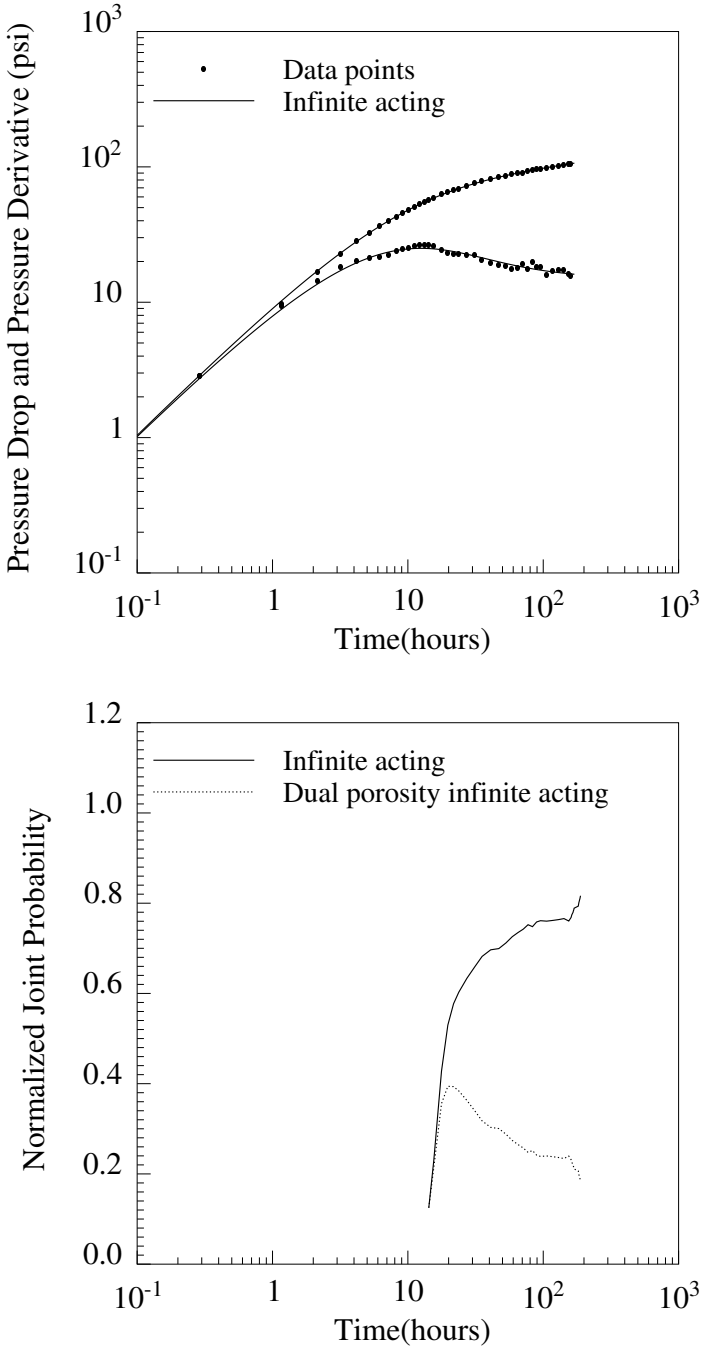

Figure 5.4: Matches to the data points (upper) and the corresponding normalized joint probability (lower) for Test 2

Table 5.9: Well and reservoir parameters for Test 3

Parameter	Value
Type of test	Buildup
Wellbore radius	0.29 ft
Porosity	0.07
Formation thickness	36 ft
Flow rate	960 bbl/day
Viscosity	1.0 cp
Formation volume factor	1.28 bbl/STB
Total compressibility	18.05×10^{-6} psi^{-1}
Initial pressure	92.32 psia
Producing time	50.75 hr

5.1.3 Test 3: Dual Porosity Response

This is a buildup test in a dual porosity reservoir. The data were obtained from Table 6-3 of the book by Sabet (1991). Table 5.9 shows the values of the well and reservoir parameters. The pressure data are shown in Table 5.10. The well was shut in for less than four hours after it had been on production for about 50 hours. The pressure derivatives and the activation levels from the neural network are plotted in Figure 5.5. The derivative plot indicates a possibility of dual porosity behavior.

The only patterns that showed up in the neural network recognition were the dip and the flat slope patterns. The dip pattern corresponds to the presence of dual porosity. The values of storativity ratio (ω) and transmissivity ratio (λ) were calculated using the minimum point of the dip pattern as described in Section 4. The values of permeability and skin were determined using the data in the flat region. The radius of investigation was used as the distance to a boundary. The initial estimates of all the reservoir parameters required by the eight reservoir models are shown in Table 5.11.

After running the sequential predictive probability program with the computed initial estimates, the normalized joint probabilities of significant values are plotted in Figure 5.6. The dual porosity sealing fault has the highest normalized joint probability

Table 5.10: Well test data for Test 3

Time (hours)	Pressure (psia)	Time (hours)	Pressure (psia)	Time (hours)	Pressure (psia)
50.7500	0.0000	50.9424	41.9750	51.7424	54.8740
50.7535	11.0950	50.9646	42.6400	51.7979	55.4470
50.7590	20.6930	50.9868	43.2810	51.8535	55.8750
50.7646	25.4000	51.0090	43.9690	51.9646	56.8450
50.7702	28.1050	51.0313	44.5420	52.0757	57.6860
50.7757	29.9780	51.0535	45.0850	52.1868	58.3430
50.7813	31.4070	51.0757	45.6580	52.2979	59.0540
50.7868	32.4990	51.1313	46.8040	52.4090	59.7260
50.7924	33.3860	51.1868	47.8360	52.5202	60.3450
50.7979	34.0960	51.2424	48.7910	52.6313	60.9490
50.8090	35.2880	51.2979	49.7000	52.7424	61.4760
50.8202	36.2130	51.3535	50.5410	52.8535	61.9950
50.8313	36.9850	51.4146	51.3050	52.9646	62.4770
50.8424	37.7180	51.4646	51.9390	53.1868	63.3630
50.8535	38.3300	51.5201	52.5890	53.4424	64.3030
50.8757	39.4150	51.5757	53.2080	53.6646	64.9830
50.8979	40.3850	51.6313	53.7960	53.8868	65.6860
50.9202	41.2110	51.6868	54.4000	54.1090	66.2290

Table 5.11: Initial estimates of reservoir parameters for Test 3

Parameter	Initial Estimate
k	251.10
S	-4.21
C	0.11
ω	0.280
λ	8.20e-06
r_e	839.12

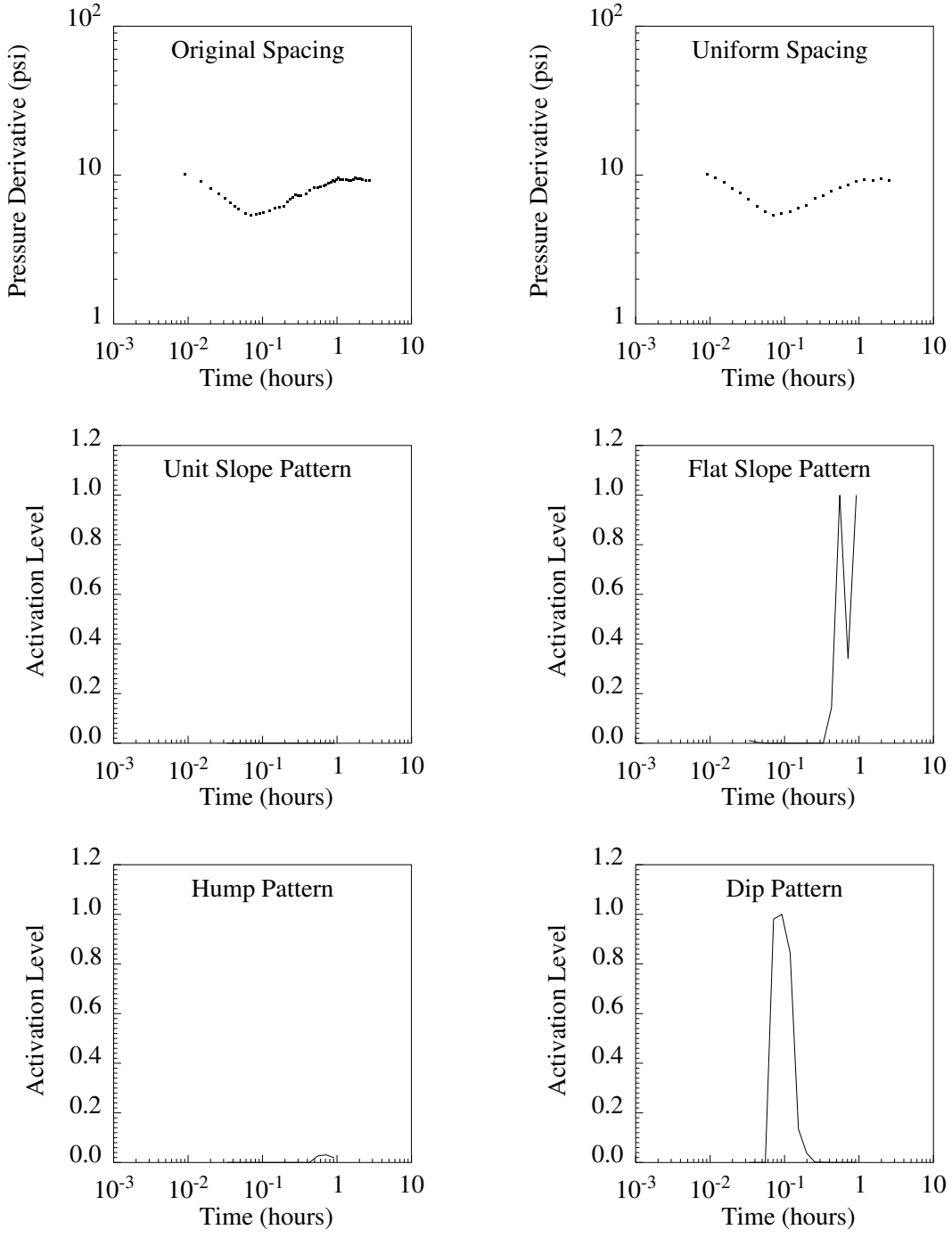

Figure 5.5: Activation levels of different patterns from neural network for Test 3

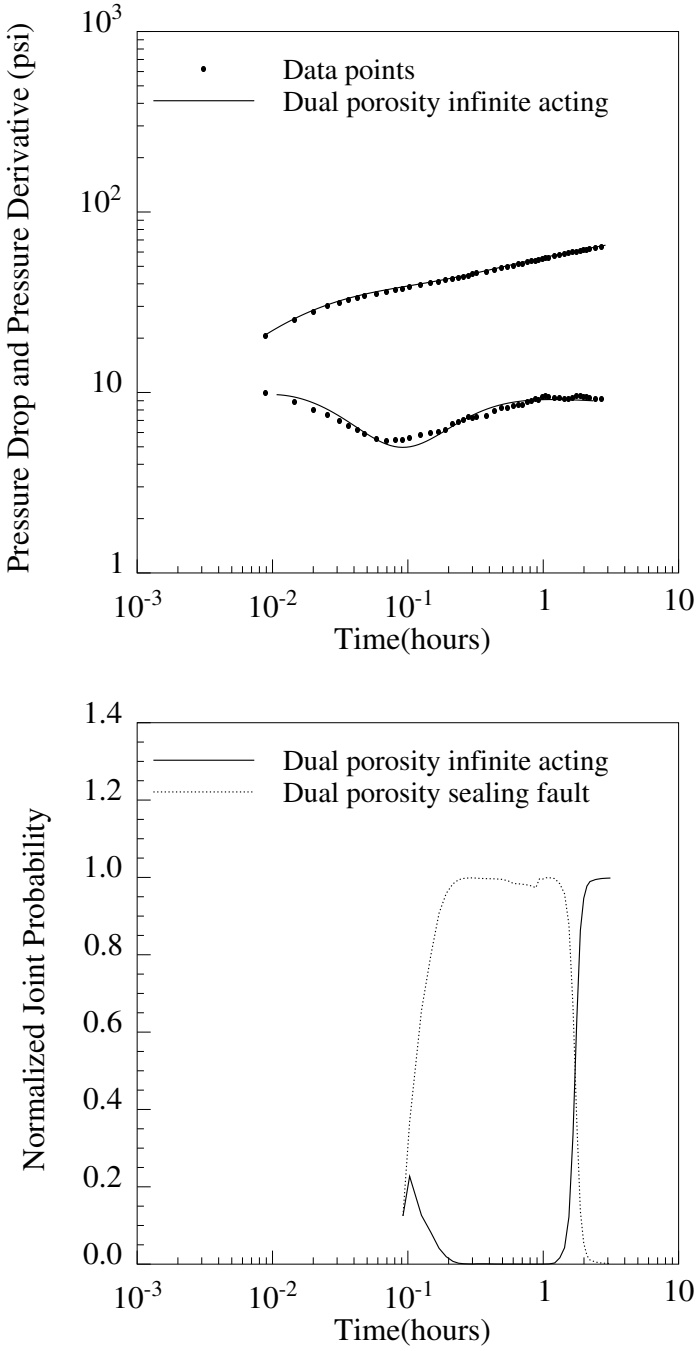

Figure 5.6: Matches to the data points (upper) and the corresponding normalized joint probability (lower) for Test 3

Table 5.12: Comparison between the initial estimates and fitted values of reservoir parameters for Test 3

Parameter	Initial Estimate	Eventual Estimate	Confidence Interval
k	251.10	255.33	$\pm$ 0.24%
S	-4.21	-4.12	$\pm$ 0.025
C	0.11	7.15e-03	$\pm$ 10.47%
ω	0.280	0.223	$\pm$ 8.47%
λ	8.20e-06	7.61e-06	$\pm$ 6.52%

at first. Then, the normalized joint probability of the dual porosity infinite acting radial flow increases while that of the dual porosity sealing fault descends. At the end of the test, the dual porosity infinite acting model has the highest normalized joint probability, and is therefore the most likely. Shown above the normalized joint probability plot is the pressure derivative with the fitted dual porosity infinite acting radial flow model curves. The initial estimates and the eventual estimates of the reservoir parameters are compared in Table 5.12. Also shown in Table 5.12 are the confidence intervals for all the parameters.

5.2 Application to Simulated Well Test Data

Several sets of simulated well test data for various types of reservoirs were used to test the application of the neural network and the sequential predictive probability method. Three of them are discussed here. The purpose in using the simulated test data is to know the answer in advance in order to be able to evaluate the effectiveness of the procedure. The test data were simulated with the corresponding analytical reservoir models with random noise.

5.2.1 Example 1: Closed Boundary Reservoir

The data for this simulated drawdown test were taken from Drawdown Example 1(a) in the book by Horne (1995). The well is produced at a constant flow rate for 72

Table 5.13: Initial estimates of reservoir parameters for Example 1

Parameter	Initial Estimate
k	77.89
S	6.23
C	0.0178
ω	0.79
λ	1.58e-07
r_e	783.0

hours. The derivative plot and the activation levels for different patterns from the neural network are shown in Figure 5.7.

An identification of the unit slope pattern at the beginning of the test by the neural network indicated that the test encounters the wellbore storage regime. Following the unit slope is the hump pattern which was identified simultaneously with the flat slope pattern. The neural network misclassified the pattern as the flat slope pattern. However, we understand that the infinite acting radial flow regime cannot occur this early. Therefore, the suggested flat slope pattern was discarded by the algorithm under the rules described earlier. When the pressure transient reaches the true infinite acting radial flow, the neural network did not recognize the flat slope pattern. This is because the region is shorter than a log cycle. However, we could still estimate the values of permeability and skin applying the procedure described in Section 4.

The neural network also identified the presence of the dip pattern. We considered this as a possibility that the reservoir may be dual porosity. The values of storativity ratio (ω) and transmissivity ratio (λ) were then computed. At the end of the test, the neural network identified the existence of another unit slope pattern. This late time unit slope corresponds to a presence of a closed boundary. The distance to the closed boundary was then determined using the procedure described in Section 4. All the initial estimates of reservoir parameters for the eight reservoir models are tabulated in Table 5.13.

The sequential predictive probability program was then run with the computed

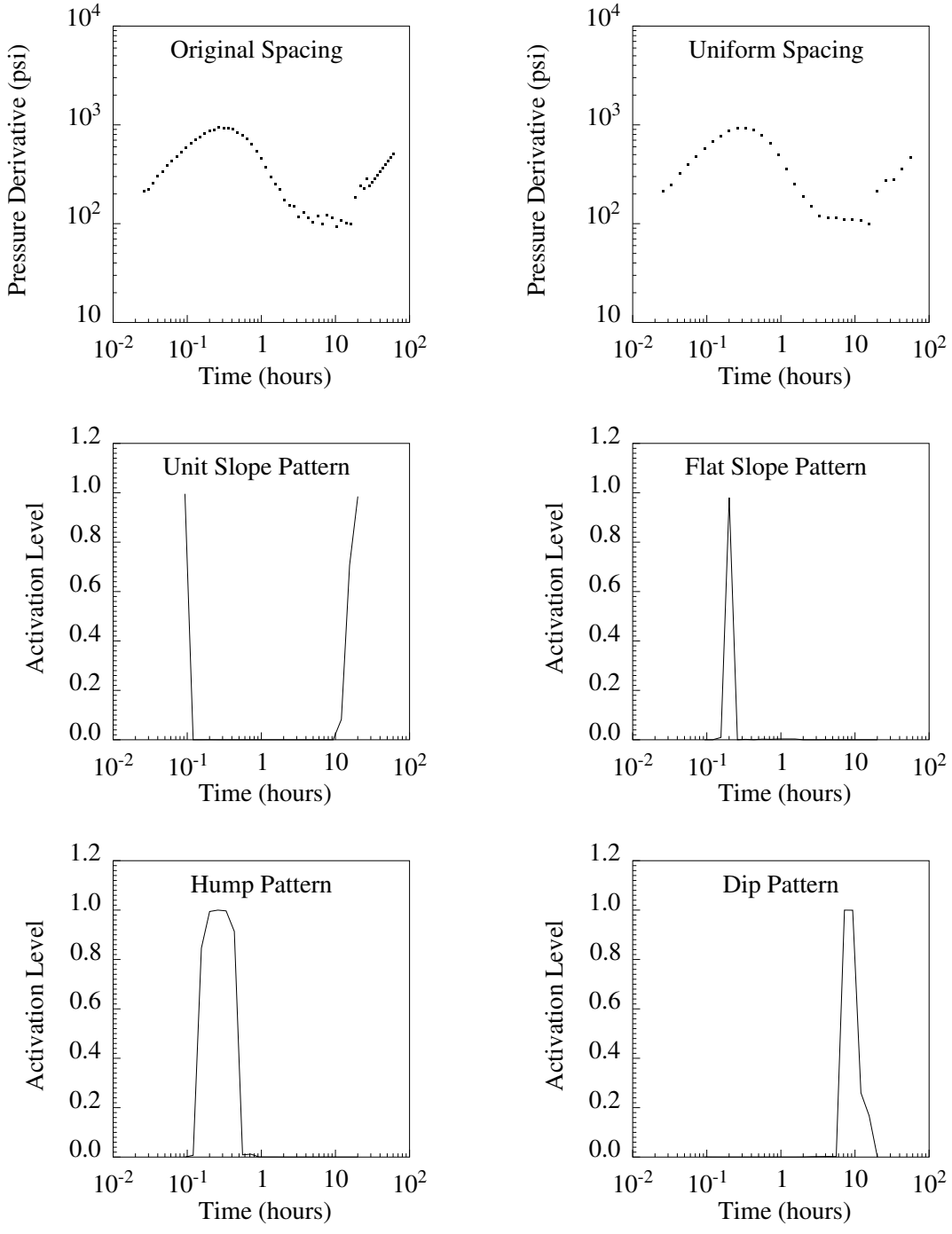

Figure 5.7: Activation levels of different patterns from neural network for Example 1

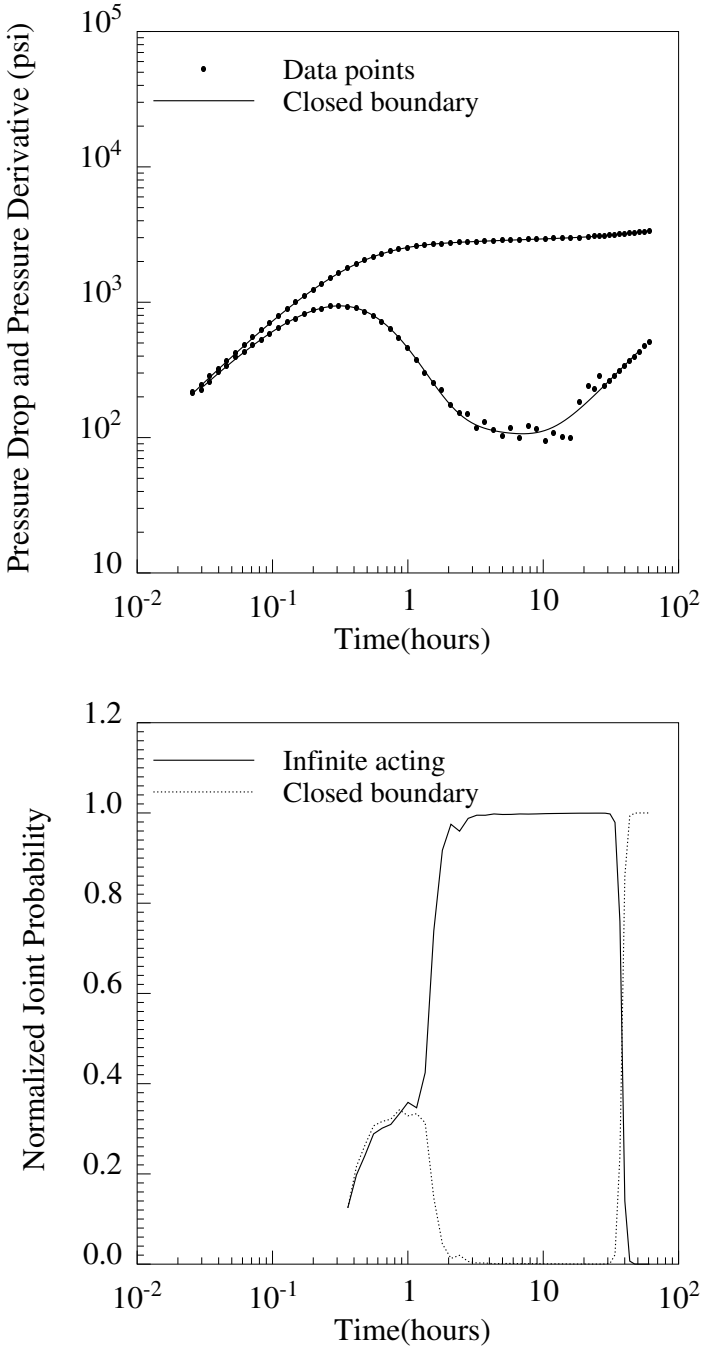

Figure 5.8: Matches to the data points (upper) and the corresponding normalized joint probability (lower) for Example 1

Table 5.14: Comparison between the initial estimates and fitted values of reservoir parameters for Example 1

Parameter	Initial Estimate	Eventual Estimate	Confidence Interval
k	77.89	88.71	$\pm$ 2.13%
S	6.23	8.04	$\pm$ 0.304
C	0.0178	0.0146	$\pm$ 0.41%
r_e	783.0	792.8	$\pm$ 0.94%

initial estimates. The normalized joint probabilities of significant values are plotted in Figure 5.8. At first when the boundary is not yet detected, the infinite acting radial flow model has the highest normalized joint probability. Then, the normalized joint probability of the closed boundary model increases and exceeds that of the infinite acting model. At the end of the test, the closed boundary reservoir model has the highest normalized joint probability. Therefore, this reservoir is correctly identified as a closed circular reservoir, which was the model used to simulate the data. Shown above the normalized joint probability plot is the derivative plot depicting the fitted curves generated from the closed boundary model.

The initial estimates and the eventual estimates of the reservoir parameters for the closed boundary model and the confidence intervals are shown in Table 5.14. The initial estimates are reasonably close to the eventual values of the parameters (which are known to be correct in this simulated test). Hence, the neural network and the parameter estimation algorithm have been found to be effective in obtaining good initial estimates for the parameter values.

5.2.2 Example 2: Fault Boundary Reservoir

The data for this drawdown test were simulated using the fault boundary reservoir model. The well is produced at a constant flow rate for 200 hours. The pressure derivative plot and the activation levels for different patterns from the neural network are shown in Figure 5.9.

The neural network indicated the presence of the unit slope pattern, the hump

Table 5.15: Initial estimates of reservoir parameters for Example 2

Parameter	Initial Estimate
k	173.94
S	1.76
C	0.0146
ω	0.60
λ	1.63e-06
r_e	576.8

pattern (which again was identified simultaneously with the flat slope pattern), the dip pattern, and finally the flat slope pattern at the end of the test. Again, the first flat slope that was identified simultaneously with the hump was discarded. Similar to the previous example, the neural network did not recognize the actual infinite acting radial flow. The flat slope at the end of the data is very late in the test (about two and a half log cycles after the end of the wellbore storage), and hence does not represent the infinite acting period. However, we could still estimate the values of permeability and skin using the procedure described earlier. The flat slope at the end of the test was, in fact, an indication of a fault boundary. The values of the derivatives of the flat region were checked if they are approximately twice those in the infinite acting region. In the program, the range of 1.5 to 2.5 was used for ratio between the average derivative of the second flat slope and that of the first flat slope. The distance to the fault boundary was then determined using the time the two semilog straight lines intersect. The neural network also identified the possibility that the reservoir is dual porosity. The values of storativity ratio (ω) and transmissivity ratio (λ) were computed using the minimum point in the dip pattern. Table 5.15 summarizes the initial estimates for all the parameters.

The sequential predictive probability program was then run with the computed initial estimates. The normalized joint probabilities of significant values are plotted in Figure 5.10. The infinite acting radial flow model has the highest normalized joint probability at first. Then, the normalized joint probability of the dual porosity infinite acting model exceeds that of the infinite acting model. Later in the test,

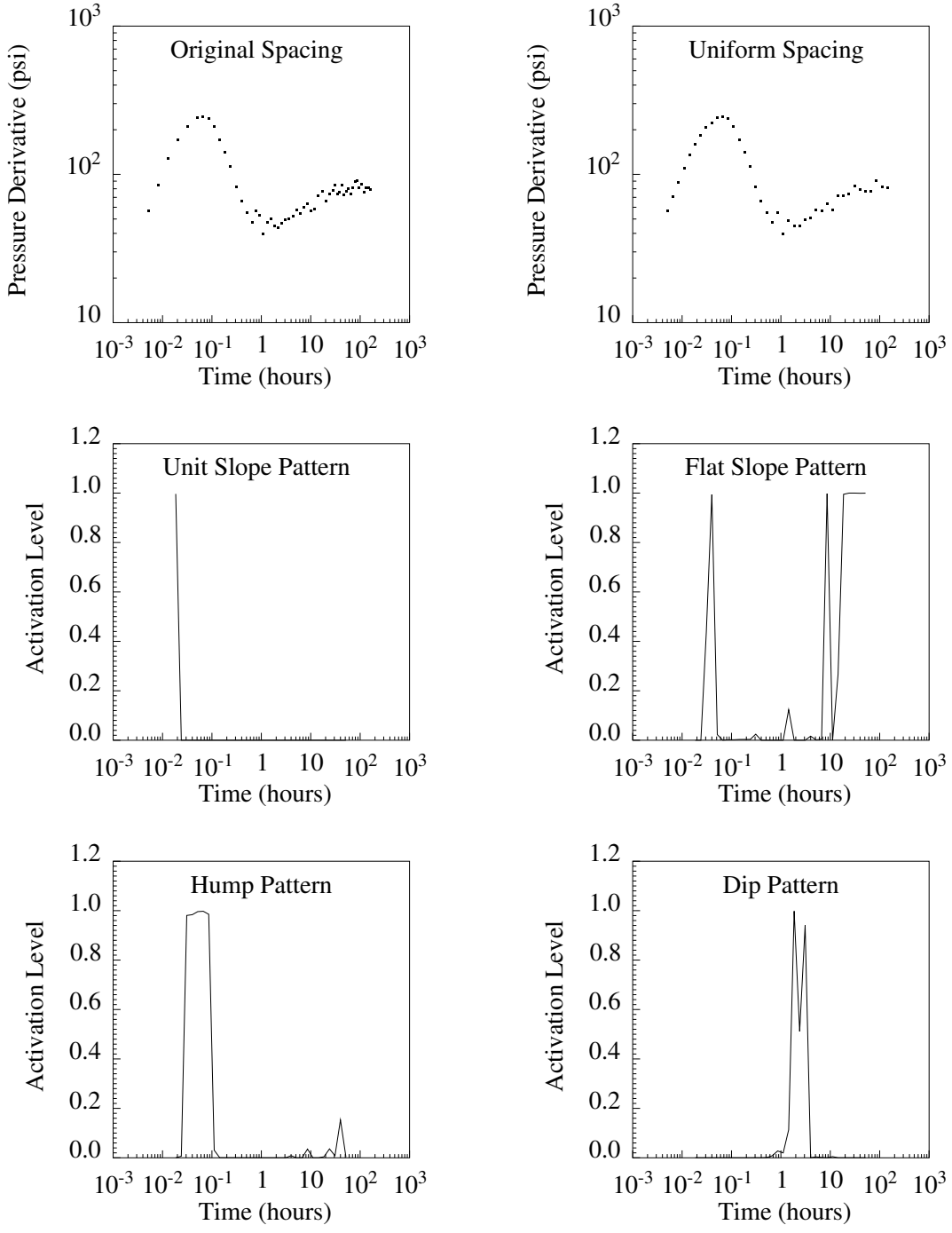

Figure 5.9: Activation levels of different patterns from neural network for Example 2

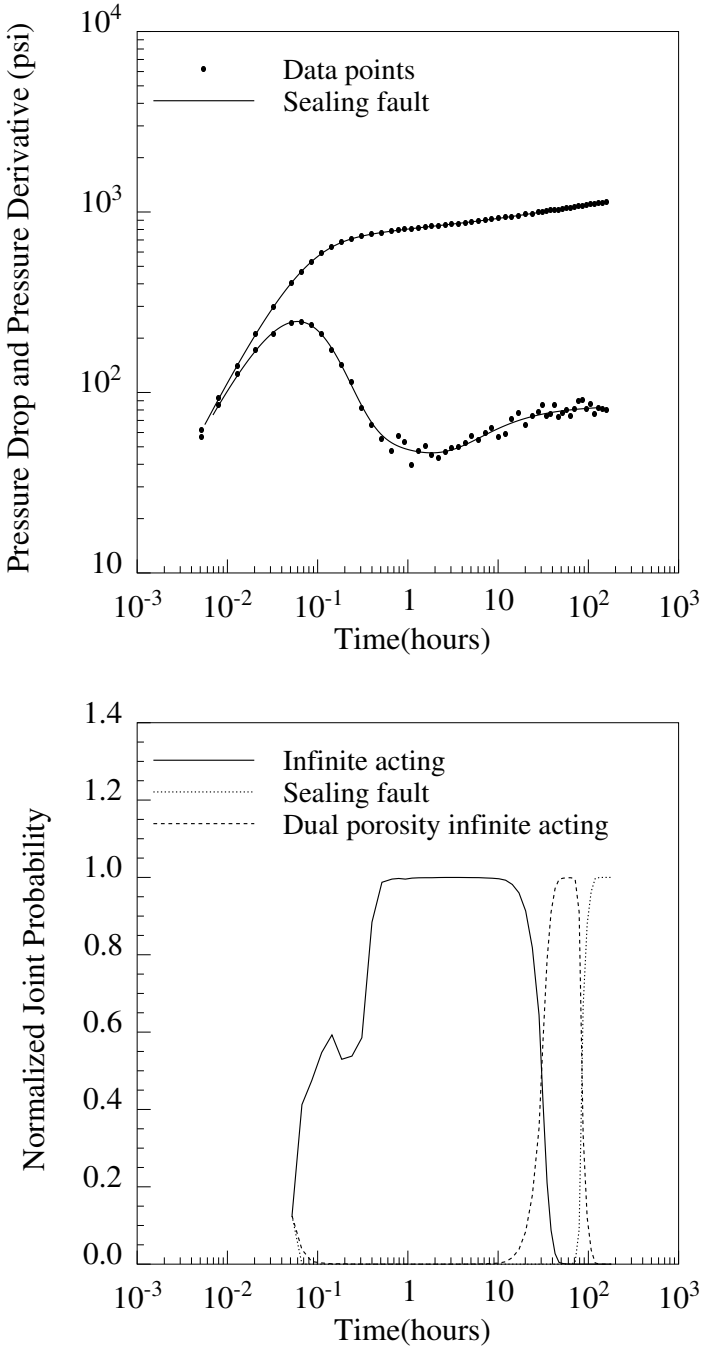

Figure 5.10: Matches to the data points (upper) and the corresponding normalized joint probability (lower) for Example 2

Table 5.16: Comparison between the initial estimates and fitted values of reservoir parameters for Example 2

Parameter	Initial Estimate	Eventual Estimate	Confidence Interval
k	173.94	201.82	$\pm$ 1.22%
S	1.76	3.07	$\pm$ 0.109
C	0.0146	0.0100	$\pm$ 0.54%
r_e	576.8	484.0	$\pm$ 3.86%

the normalized joint probability of the sealing fault model increases and becomes the highest. This reservoir is most likely a fault boundary reservoir, which was the model used in simulating the data. Shown above the normalized joint probability plot in Figure 5.10 is the pressure derivative with the fitted curves generated from the sealing fault model. The initial estimates and the eventual estimates from the sequential predictive probability program for the closed boundary model are compared in Table 5.16.

5.2.3 Example 3: Constant Pressure Boundary Reservoir

A drawdown test in a constant pressure boundary reservoir was simulated for approximately 75 hours. The pressure derivative plot and the activation levels for different patterns from the neural network are shown in Figure 5.11. The neural network identified the presence of the hump pattern (simultaneously with the flat slope pattern), the descending pattern immediately after the hump, and the second descending pattern at the end of the test. Again, the flat slope that was identified simultaneously with the hump was discarded. The neural network did not recognize the actual infinite acting radial flow due to the short period of the flat region. The descending pattern at the end of the data for a drawdown test indicated the presence of a constant pressure boundary. The values of the pressures at the descending log cycles identified by the neural network were checked if they are approximately constant. In this case, they are relatively constant. The distance to the constant pressure boundary was determined applying the procedure described in Section 4. Table 5.17 summarizes

Table 5.17: Initial estimates of reservoir parameters for Example 3

Parameter	Initial Estimate
k	66.77
S	2.50
C	0.0129
ω	0.99
λ	0.99
r_e	961.5

Table 5.18: Comparison between the initial estimates and fitted values of reservoir parameters for Example 2

Parameter	Initial Estimate	Eventual Estimate	Confidence Interval
k	66.77	70.09	$\pm$ 0.81%
S	2.50	3.01	$\pm$ 0.078
C	0.0129	0.0100	$\pm$ 0.33%
r_e	961.5	1001.8	$\pm$ 1.65%

the initial estimates for all the reservoir parameters.

We then entered the computed initial estimates into the sequential predictive probability program. The normalized joint probabilities of significant values are plotted in Figure 5.12. The normalized joint probability of the constant pressure boundary model is the highest at the end of the test. This reservoir is most likely a constant pressure circular reservoir, which was the model used in simulating the data. Shown above the normalized joint probability plot is the pressure derivative with the fitted constant pressure boundary curves. The initial estimates and the eventual estimates of the reservoir parameters from the sequential predictive probability program are compared in Table 5.18.

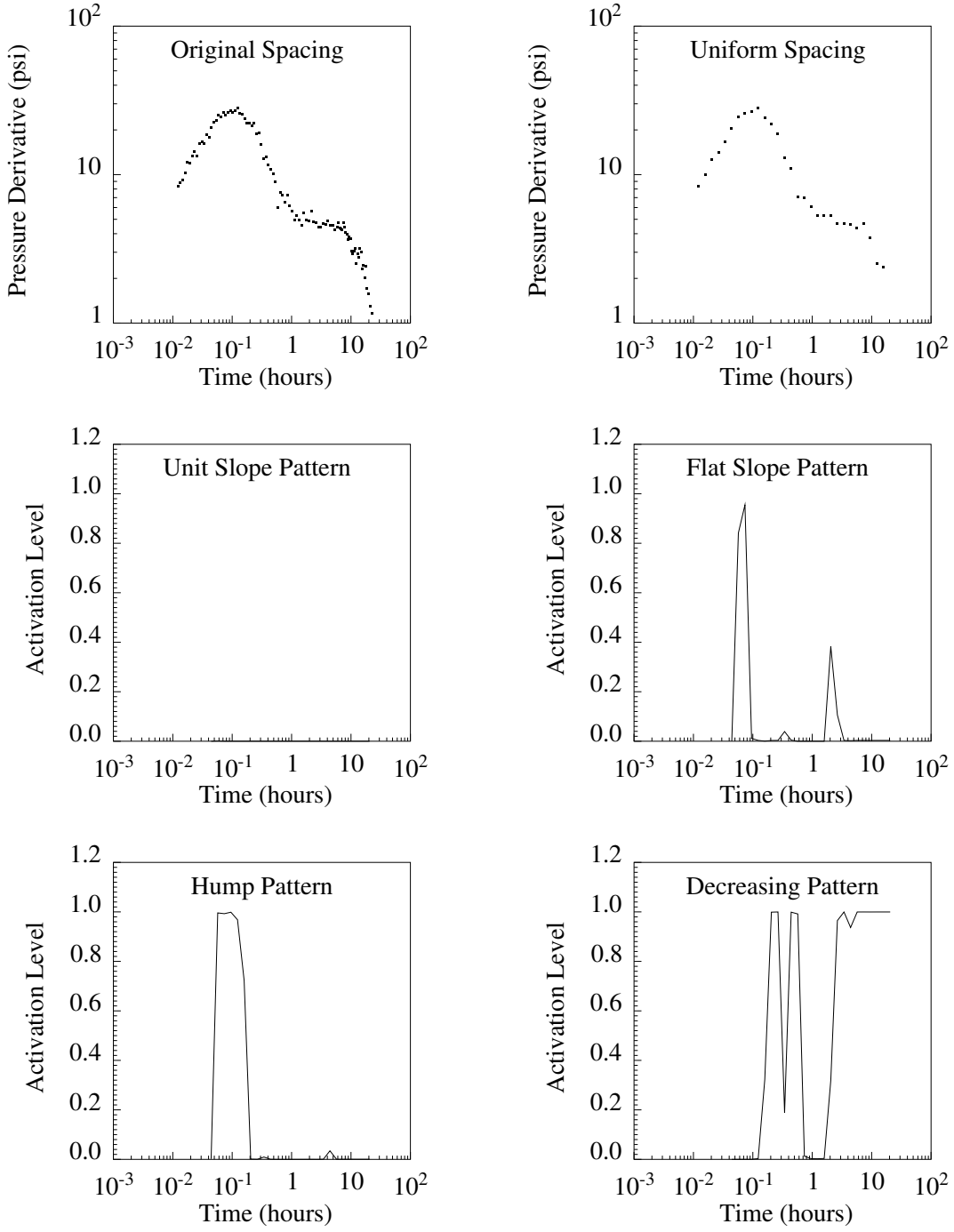

Figure 5.11: Activation levels of different patterns from neural network for Example 3

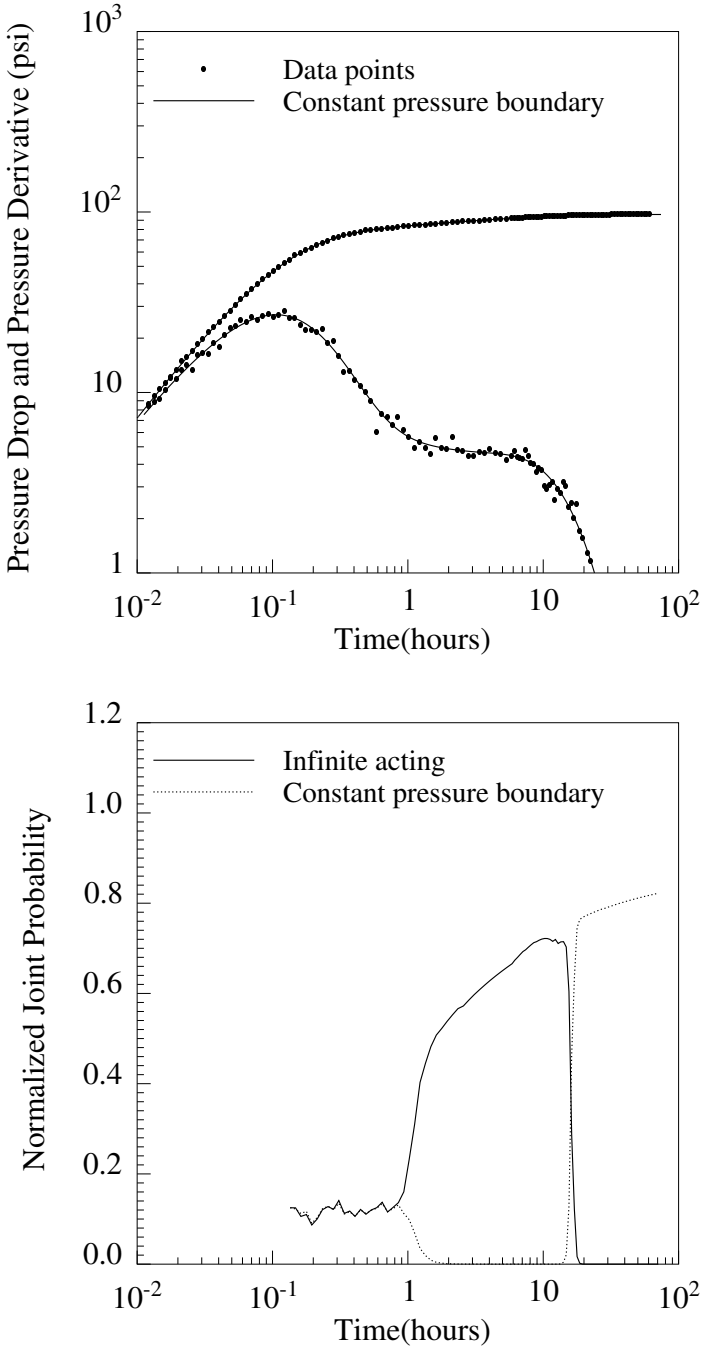

Figure 5.12: Matches to the data points (upper) and the corresponding normalized joint probability (lower) for Example 3

Section 6

Conclusion

We investigated the implementation of a procedure that combined the artificial neural network approach and the sequential predictive probability method to mechanize well test interpretation. The artificial neural network was used to classify the characteristic components of the pressure derivative curve. The signals obtained from the neural network were then transformed into a description of reservoir flow regimes. Initial estimates of reservoir parameters were made using the data in the relevant flow regimes and used as initial guesses in the sequential predictive probability program which discriminates between reservoir models and obtains the best estimates of the models' parameters.

Several remarks can be from our experience in applying this approach:

1. The neural network is tolerant to noise in the data. This property provides both advantage and disadvantage. The neural network is effective in recognizing noisy data, and data smoothing was not found necessary. However, the method sometimes recognized something else similar but not actually belonging to a pattern. Introducing the knowledge of well test interpretation into the algorithm was useful in eliminating false classification.

2. The neural network trained in this work had a clear weakness in identifying the flat slope pattern. This problem was overcome by integrating our knowledge of well test interpretation into the algorithm that extracts the flow regime

description from the neural network's signals. If another neural network with a distinctive weakness is used, the procedure used to identify the correct flow regimes from the neural network's signals may be different from the one in this work.

3. The sequential predictive probability method was generally successful in identifying the reservoir model.

4. This approach provides a new way to speed up interpretation of well test data. It is a further step toward full automation of computer-aided well test interpretation. A similar procedure should also be useful for fully automated oversight of permanent downhole gauges.

5. The number of reservoir models used in this work was limited. Fullly mechanized interpretation would require the neural network to identify several more characteristic components from the pressure derivative plot and the provision a larger number of reservoir models in the sequential predictive probability program.

6. Geological, well log, and other information should be fully explored and incorporated with the interpretation. This can be included as an additional step in the process in which candidate models are selected based on their consistency with available geological and other information.

Nomenclature

A	=	Reservoir area, ft^2
B	=	Formation volume factor, $res\ vol/std\ vol$
C	=	Wellbore storage coefficient, STB/psi
C_A	=	Shape factor, $dimensionless$
c_t	=	Total system compressibility, psi^{-1}
d	=	Distance to fault boundary, ft
h	=	Thickness, ft
k	=	Permeability, md
m	=	Slope of the semilog plot, psi
$m_{Cartesian}$	=	Slope of the Cartesian plot, psi/hr
net	=	Input, $dimensionless$
O	=	Calculated output, $dimensionless$
p_{1hr}	=	Pressure at time 1 hour extrapolated from the fitted straight line , psi
p_D	=	Dimensionless pressure
p_i	=	Initial reservoir pressure, psi
p_{wf}	=	Well flowing pressure, psi
p_{ws}	=	Shutin pressure, psi
q	=	Production rate, STB/D
r_e	=	Distance to outer boundary, ft
r_{inv}	=	Radius of investigation, ft
r_w	=	Wellbore radius, ft

S = Skin factor, *dimensionless*

t = Time, *hrs*

t_D = Dimensionless time, *dimensionless*

t_p = Producing time, *hrs*

t_x = Time at which two semilog straight lines intersect, *hrs*

w = Weight, *dimensionless*

GREEK LETTERS

α = Slope from the plot of pressure change versus time, psi/hr

λ = Transmissivity ratio, *dimensionless*

Δ = Difference

μ = Viscosity, *cp*

ϕ = Porosity, *dimensionless*

ω = Storativity ratio, *dimensionless*

SUBSCRIPT

D = Dimensionless

i, j = Integer indices (layer i and layer j)

ji = Integer indices (between layer i and layer j)

new = New iteration

old = Old iteration

Bibliography

[1] Al-Kaabi, A.U. and Lee, W.J.: "Using Artificial Neural Networks to Identify the Well Test Interpretation Model," paper SPE 20332 presented at the 1990 SPE Petroleum Computer Conference, Denver, CO, June 25-28.

[2] Allain, O.F. and Horne, R.N.: "Use of Artificial Intelligence in Well Test Analysis," *JPT* (March 1990) 342–349.

[3] Allain, O.F. and Houzé, O.P.: "A Practical Artificial Intelligence Application in Well Test Interpretation," paper SPE 24287 presented at the 1992 SPE European Petroleum Computer Conference, Stavanger, Norway, May 25-27.

[4] Anraku, T.: *Discrimination Between Reservoir Models in Well Test Analysis*, PhD dissertation, Stanford University (December 1993).

[5] Anraku, T. and Horne, R.N.: "Discrimination Between Reservoir Models in Well Test Analysis," paper SPE 26426 presented at the 1993 SPE Annual Technical Conference and Exhibition, Houston, TX, October. To appear in SPEFE.

[6] Beale, R. and Jackson, T.: *Neural Network: An Introduction*, Institute of Physics Publishing (1990).

[7] Bourdet, D., Ayoub, J.A. and Pirard, Y.M.: "Use of Pressure Derivative in Well Test Interpretation," paper SPE 12777 presented at the 1984 California Regional Meeting, Long Beach, CA, April 11-13.

[8] Bourdet, D., Ayoub, J.A. and Pirard, Y.M.: "Use of Pressure Derivative in Well-Test Interpretation," *SPEFE* (June 1989) 293–302.

[9] Bourdet, D., Whittle, T.M., Douglas, A.A. and Pirard, Y.M.: "A New Set of Type Curves Simplifies Well Test Analysis," *World Oil* (May 1983a) 95–106.

[10] Bourdet, D., Whittle, T.M., Douglas, A.A., Pirard, Y.M. and Kniazeff, V.J.: "Interpreting Well Tests in Fractured Reservoirs," *World Oil* (Oct. 1983b) 95–106.

[11] Davis, E.G., Jr. and Hawkins, M.F., Jr.: "Linear Fluid-Barrier Detection by Well Pressure Measurements," *J. Pet. Tech* (October 1963) 1077–1079.

[12] Economides, M.J., Hill, A.D., and Ehlig-Economides, C.: *Petroleum Production Systems*, Prentice Hall (1994).

[13] Ershaghi, I., Li, X. and Hassibi, M.: "A Robust Neural Network Model for Pattern Recognition of Pressure Transient Test Data," paper SPE 26427 presented at the 1993 SPE Annual Technical Conference and Exhibition, Houston, TX, October 3-6.

[14] Fausett: *Fundamentals of Neural Networks*, Prentice Hall International, Inc. (1994).

[15] Gray, K.E.: "Approximating Well-to-Fault Distance from Pressure Build-Up Tests," *J. Pet. Tech* (July 1965) 761–767.

[16] Horne, R.N.: "Advances in Computer-Aided Well Test Interpretation," *J. Pet. Tech* (July 1994) 559–606.

[17] Horne, R.N.: *Modern Well Test Analysis: A Computer-Aided Approach*, Petroway, Inc., 2nd edition (1995).

[18] Lee, R.L.: *Well Testing*, SPE Dallas, TX; SPE Textbook Series, No. 1 (1982).

[19] Regier, T.: *Computer Program: NevProp*, unssun.scs.unr.edu: /pub /goodman /nevpropdir (1993).

[20] Sabet, M.: *Well Test Analysis*, Gulf Publishing (1991).

[21] Wasserman, P.: *Neural Computing: Theory and Practice*, Van Nostrand Reinhold, New York (1989).